Article

SOURCE DATA | TRANSPARENT PROCESS

THE EMBO JOURNAL

Reduced pachytene piRNAs and translation underlie spermiogenic arrest in Maelstrom mutant mice

Julio Castañeda[1,2,†], Pavol Genzor[1,2], Godfried W van der Heijden[2], Ali Sarkeshik[3], John R Yates III[3], Nicholas T Ingolia[2,*,‡] & Alex Bortvin[2,**]

Abstract

Pachytene piRNAs are a class of Piwi-interacting small RNAs abundant in spermatids of the adult mouse testis. They are processed from piRNA primary transcripts by a poorly understood mechanism and, unlike fetal transposon-derived piRNAs, lack complementary targets in the spermatid transcriptome. We report that immunopurified complexes of a conserved piRNA pathway protein Maelstrom (MAEL) are enriched in MIWI (Piwi partner of pachytene piRNAs), Tudor-domain proteins and processing intermediates of pachytene piRNA primary transcripts. We provide evidence of functional significance of these complexes in *Mael*^{129} knockout mice that exhibit spermiogenic arrest with acrosome and flagellum malformation. *Mael*^{129}-null mutant testes possess low levels of piRNAs derived from MAEL-associated piRNA precursors and exhibit reduced translation of numerous spermiogenic mRNAs including those encoding acrosome and flagellum proteins. These translation defects in haploid round spermatids are likely indirect, as neither MAEL nor piRNA precursors associate with polyribosomes, and they may arise from an imbalance between pachytene piRNAs and MIWI.

Keywords germ cell; maelstrom; mouse; piRNA; Piwi
Subject Categories Development & Differentiation; Protein Biosynthesis & Quality Control; RNA Biology
DOI 10.15252/embj.201386855 | Received 10 September 2013 | Revised 12 June 2014 | Accepted 2 July 2014 | Published online 25 July 2014
The EMBO Journal (2014) 33: 1999–2019

See also: **RR Pandey & RS Pillai** (September 2014)

Introduction

Piwi proteins and associated piRNAs play a well-documented role in protecting genomes of metazoan germ cells from deleterious consequences of transposon mobilization (Siomi *et al*, 2011). Genomic origins, biogenesis, and functioning of mammalian piRNAs have been extensively explored in the context of male germ cell differentiation in mice (Aravin & Bourc'his, 2008; Pillai & Chuma, 2012). Fetal, meiotic, and post-meiotic male germ cells express overlapping, but nonetheless distinct populations of piRNAs (Aravin *et al*, 2006, 2007b, 2008; Girard *et al*, 2006; Grivna *et al*, 2006a; Watanabe *et al*, 2006; Kuramochi-Miyagawa *et al*, 2008). The current understanding of murine piRNAs comes from studies of the fetal population that is enriched in sequences targeting various classes of transposable elements populating the mouse genome (Aravin *et al*, 2008; Kuramochi-Miyagawa *et al*, 2008). Abrogation of piRNA production by mutating genes for two Piwi proteins expressed in fetal germ cells, *Mili/Piwil2,* and *Miwi2/Piwil4* results in deficient *de novo* DNA methylation of transposable elements and eventual demise of the adult meiotic cell population (Kuramochi-Miyagawa *et al*, 2004, 2008; Aravin *et al*, 2007b; Carmell *et al*, 2007). The need for the silencing of transposons, such as the retrotransposon LINE-1 (L1), arises from the process of epigenetic reprogramming of germ cell genomes during the early phase of their differentiation (Bourc'his & Bestor, 2004; Aravin & Bourc'his, 2008; Lees-Murdock & Walsh, 2008).

Fetal piRNAs are produced either by a primary mechanism that is independent of the preexisting piRNAs or by a feed-forward secondary process that is guided by already existing primary piRNAs (Aravin *et al*, 2007a, 2008; Aravin & Bourc'his, 2008). In contrast to fetal piRNAs, derived from sense or anti-sense transposon transcripts, a highly abundant population of primary piRNAs of the adult testis is generated from 100 long non-coding RNAs whose transposon content is below the genomic average (Li *et al*, 2013a,b). A lack of clear target specificity of these piRNAs, coined "pachytene" to reflect the initial stage of their expression, has led to various proposals ranging from functions in meiotic chromosome organization to not having a function at all (Girard *et al*, 2006; Vourekas *et al*, 2012). It is without any doubt, however, that the

1 Department of Biology, Johns Hopkins University, Baltimore, MD, USA
2 Department of Embryology, Carnegie Institution for Science, Baltimore, MD, USA
3 Department of Chemical Physiology, The Scripps Research Institute, La Jolla, CA, USA
*Corresponding author. Tel: +1 510 664 7071; E-mail: ingolia@berkeley.edu
**Corresponding author. Tel:+1 410 246 3034; Fax: +1 410 243 6311; E-mail: bortvin@ciwemb.edu
†Present address: Department of Pathology, Baylor College of Medicine, Houston, TX, USA
‡Present address: Department of Molecular and Cell Biology, University of California, Berkeley, CA, USA

principle Piwi protein expressed at that stage, MIWI/PIWIL1, is essential for differentiation of haploid round spermatids (spermiogenesis) which, by analogy with MILI and MIWI2, implies that pachytene piRNAs are functionally relevant (Deng & Lin, 2002). Pachytene piRNAs require extensive complementarity to guide mRNA slicing by MIWI, which appears to be an inefficient nuclease, but whether same is true for translational repression by MIWI is not known (Reuter *et al*, 2011; Vourekas *et al*, 2012). Early analysis of MIWI suggested its association both with translationally inactive mRNAs and polysomes (Grivna *et al*, 2006b). A more recent study demonstrated that MIWI binds mRNAs in a piRNA-independent manner (Vourekas *et al*, 2012). This finding provides a way to explain the demise of *Miwi*-mutant round spermatids as a consequence of altered mRNA stability and/or translation, and to dissociate the germ cell-phenotype from pachytene piRNAs altogether. But this explanation does not fully account for mutant phenotypes observed in mice with catalytically inactive MIWI including upregulation of L1 expression and accumulation of DNA damage in round spermatids (Reuter *et al*, 2011). Therefore, it is possible that the minority of pachytene piRNAs complementary to transposons represent the functional arm of the piRNA system, while pachytene piRNA precursor genes have a role of large genomic sinks that capture new transposition events to protect the spermatid genome (Zheng & Wang, 2012). Recent studies have also suggested a role for pachytene piRNAs in stimulating MIWI turnover in late spermiogenesis further strengthening the argument for a function for this abundant class of piRNAs (Zhao *et al*, 2013).

In addition to PIWI proteins and piRNAs, normal biogenesis and function of piRNAs require numerous additional evolutionarily conserved proteins including several Tudor-domain proteins, a putative endonuclease MitoPLD/Zucchini, helicase Mov10L1, GASZ, and others (Chuma *et al*, 2003, 2006; van der Heijden & Bortvin, 2009a; Ma *et al*, 2009; Reuter *et al*, 2009; Shoji *et al*, 2009; Huang *et al*, 2011; Watanabe *et al*, 2011; Yabuta *et al*, 2011; Ipsaro *et al*, 2012; Nishimasu *et al*, 2012; Pek *et al*, 2012; Zheng & Wang, 2012; Saxe *et al*, 2013). To further understand piRNAs in the mouse testis, we study Maelstrom (MAEL), a conserved HMG-box domain protein implicated in piRNA function and transposon control in flies and mice (Soper *et al*, 2008; Aravin *et al*, 2009; Pek *et al*, 2009; Sienski *et al*, 2012). Previously, we have shown that MAEL is expressed in fetal prospermatogonia where it co-localizes with MIWI2, TDRD9, and the mRNA degradation machinery in cytoplasmic germinal granules, piP-bodies (Aravin *et al*, 2009). $Mael^{-/-}$ fetal prospermatogonia fail to localize MIWI2 to piP-bodies and exhibit delayed and reduced production of MIWI2-bound piRNAs. MAEL is also expressed in the adult testis particularly in late spermatocytes and spermatids where it localizes to the cytoplasm and accumulates in chromatoid bodies, presumptive centers of RNA processing functionally related to piP- and pi-bodies of fetal prospermatogonia (Soper *et al*, 2008). $Mael^{-/-}$ spermatocytes of mice in the C57Bl6/J genetic background accumulate non-meiotic DNA damage and fail to synapse homologous chromosomes. These defects are thought to activate the meiotic prophase I checkpoint leading to apoptosis and arrest of spermatogenesis before the completion of meiosis. In this work, we set out to further understand the piRNA pathway in adult mouse testis by identifying MAEL-associated proteins and RNAs, and subsequently by studying novel spermatogenic phenotypes in the *Mael*-mutant 129SvJae strain of mice.

Results

piRNA pathway and chromatoid body proteins associate with MAEL

MAEL has a conserved role in transposon silencing in the germ line (Findley *et al*, 2003; Soper *et al*, 2008; Sienski *et al*, 2012); however, its biochemical function remains unknown (Zhang *et al*, 2008). Prior analysis of MIWI- and MILI-associated proteomes in the mouse testis has identified MAEL in the context of piRNA pathway machinery (Vagin *et al*, 2009), yet the MAEL-associated proteome in fly ovaries lacked piRNA pathway proteins altogether (Sato *et al*, 2011). To further understand the role of MAEL in spermatogenesis, we set out to characterize the MAEL-associated proteome in adult wild-type mouse testis. We performed mass spectrometric (MS) analysis of proteins of co-immunoprecipitating specifically with MAEL from testicular protein lysates of wild-type but not $Mael^{-/-}$ mice (Fig 1A). To control for the specificity of immunoprecipitation, we used testes of $Mael^{-/-}$ males backcrossed to the 129SvJae (129) strain of mice. As will be shown below, $Mael^{129-/-}$ testes of mutants contain not only meiotic cells but also post-meiotic spermatids and therefore are a better control than the previously described $Mael^{-/-}$ C57Bl6/J (B6) mice (Soper *et al*, 2008). Comparison of proteins identified in wild-type and $Mael^{129}$-mutant control samples uncovered 139 candidate proteins comprising the MAEL-associated proteome (Supplementary Table S1). Of those, MAEL was the most extensively represented protein with 82.5% percent coverage. In agreement with MAEL localization to germinal granules and its role in the piRNA pathway (Soper *et al*, 2008; Aravin *et al*, 2009), we identified MIWI/PIWIL1 (41.3% coverage), Tudor-repeat-domain proteins TDRD6 (62.9%), TDRD4/RNF17 (33.9%), TDRD1 (24.3%), STK31/TDRD8 (10.3%) and TDRD9 (8.8%) in the MAEL-associated proteome (Deng & Lin, 2002; Pan *et al*, 2005; Chuma *et al*, 2006; Hosokawa *et al*, 2007; Kojima *et al*, 2009; Reuter *et al*, 2009, 2011; Shoji *et al*, 2009; Vasileva *et al*, 2009). We also detected a second Piwi protein expressed in adult mouse testis, MILI, although, compared to MIWI, at a lower percent coverage (4.5%). Despite the presence of common Piwi and Tudor-domain proteins, the MAEL-associated proteome was nonetheless distinct from those reported for MIWI- and MILI-associated proteomes (Vagin *et al*, 2009). For example, only one of 10 presumptive RNA helicases identified in MIWI complexes was identified in MAEL-associated proteome (DDX25). Notably, we did not detect MVH/DDX4 RNA helicase in MAEL complexes. Likewise, symmetric methyl transferase complex proteins PRMT5 and WDR77 were absent in the MAEL-associated proteome (Vagin *et al*, 2009). At the same time, the MAEL-associated proteome contained proteins implicated in RNA modification or metabolism [ADAD1 (42.2% coverage), ADAD2 (41.2%), DDX25 (18.8%), DDX3L (16.1%)], and, in agreement with studies in *Drosophila*, the cytoskeletal network [TUBA8 (40.8%) DYL2 (39.3%), DYNLT1 (36.6%), TCTEX1 (33.3%), TBB6 (23%), PROF2 (20.7%), ACTL7A (8.2%)] (Supplementary Table S1). These results suggest that the MAEL-associated proteome identified by us was not a reproduction of MIWI or MILI proteomes but reflected on a different set of protein–protein interactions of MAEL in adult testis.

The identification of MIWI and Tudor-domain proteins in the MAEL-associated proteome is consistent with their known localization to the chromatoid body of round spermatids (Chuma *et al*,

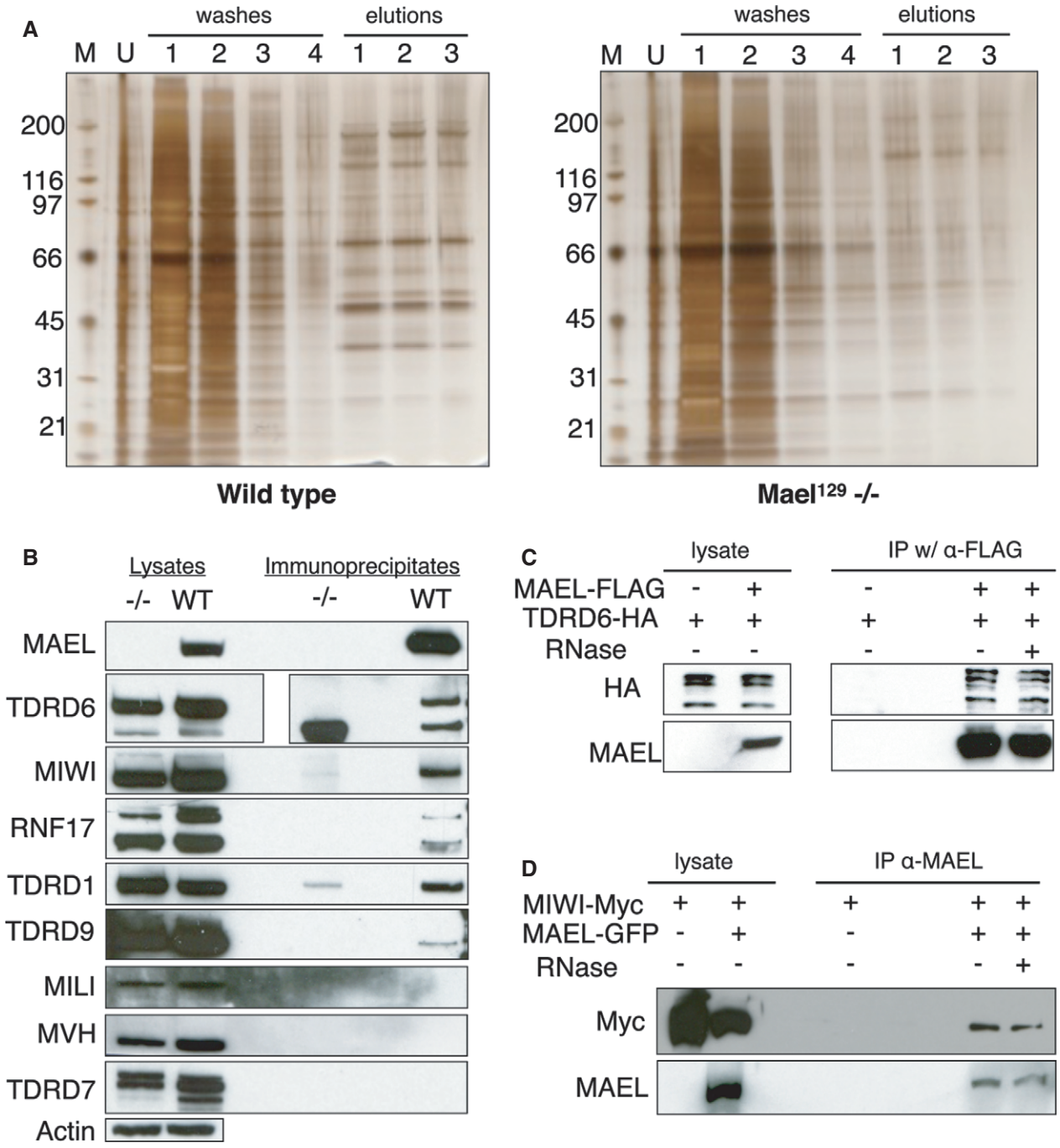

Figure 1. MAEL associates with piRNA pathway proteins.

A Silver-stained gels of proteins immunoprecipitated with anti-MAEL antibodies from WT and *Mael*$^{129-/-}$ adult testes. M, molecular weight marker; U, unbound material.

B Western blot validation of MAEL association with piRNA pathway proteins.

C Western blot analysis of immunoprecipitated proteins from lysates generated from HEK293T-cultured cells transfected with HA-tagged TDRD6 alone or co-transfected with TDRD6-HA and FLAG-tagged MAEL. Immunoprecipitations were performed in the presence or absence of RNase A.

D Western blot analysis of immunoprecipitated proteins from lysates generated from HEK293T cells either transfected with Myc-tagged MIWI alone or co-transfected with MIWI-Myc and GFP-tagged MAEL. IPs were done in the presence or absence of RNase A.

Source data are available online for this figure.

2003; Pan *et al*, 2005; Kotaja *et al*, 2006; Hosokawa *et al*, 2007). We substantiated this point further by showing MAEL co-localization with TDRD1 and TDRD6 proteins (Supplementary Fig S1). We also confirmed on Western blots co-immunoprecipitation from adult mouse testicular lysates of MAEL with MIWI, TDRD6, RNF17/TDRD4, TDRD1, and TDRD9 proteins but not with MILI (Fig 1B). In

light of prior reports of MVH co-immunoprecipitation with TDRD6 and MIWI (Vagin *et al*, 2009; Vasileva *et al*, 2009), we also probed for but did not detect this RNA helicase and universal marker of germ cells in MAEL immunoprecipitates by Western blots (Fig 1B) (Abe & Noce, 1997; Kuramochi-Miyagawa *et al*, 2010). Absence of MVH in the MAEL-associated proteome indicated by both MS and Western blot suggested that MAEL-enriched complexes containing TDRD6 and MIWI are deficient in MVH RNA helicase. In contrast to a prior report (Costa *et al*, 2006), we did not identify TDRD7 protein (Tanaka *et al*, 2011) in MAEL immunoprecipitates by MS and Western blot (Fig 1B). Consistent with these data, we observed that TDRD7 and MAEL localize to adjacent but different domains within the chromatoid body (Supplementary Fig S1).

To assess MAEL interactions with TDRD6 and MIWI proteins in the absence of piRNA production, we used the heterologous human embryonic kidney (HEK) 293T cell line (Vagin *et al*, 2009). We transfected appropriate combinations of plasmids expressing MAEL-FLAG, TDRD6-HA, MAEL-GFP, and MIWI-MYC fusion proteins into HEK293T cells and immunoprecipitated proteins of interest using specific antibodies. We observed specific co-immunoprecipitation of TDRD6-HA with MAEL-FLAG from a HEK293T cell lysates incubated with anti-FLAG antibody (Fig 1C). The interaction of MAEL with TDRD6 was unaffected by treatment of cell lysates with RNase A prior to immunoprecipitation. Likewise, we detected specific, RNA-independent association of MIWI-MYC fusion protein with MAEL-GFP following immunoprecipitation with anti-MAEL antibody (Fig 1D). Since HEK293T cells are of human somatic origin, do not express piRNA pathway proteins, and do not load Piwi proteins with piRNAs, the simplest explanation of these findings is that MAEL interacts directly with TDRD6 and MIWI (Vagin *et al*, 2009; Vasileva *et al*, 2009). At the same time, using a similar experimental approach, we determined that MAEL does not interact directly with RNF17 protein (Pan *et al*, 2005) (Supplementary Fig S2).

Since some Tudor domains recognize symmetrically dimethylated arginines (sDMA) on Piwi proteins (Kirino *et al*, 2010; Vourekas *et al*, 2010; Pek *et al*, 2012), we asked whether MAEL carried this modification. We probed MAEL and MILI proteins (immunoprecipitated from testicular protein lysates with their respective polyclonal antibodies) with the sDMA-specific antibody Y12 (Lerner *et al*, 1981). Consistent with prior reports, we readily observed sDMA on immunoprecipitated MILI but not MAEL (Supplementary Fig S3). These results suggest that MAEL interacts with TDRD6 in an RNA- and sDMA-independent manner.

MAEL associates with piRNA precursors

The identification of proteins involved in piRNA biogenesis and RNA metabolism in the MAEL-associated proteome prompted us to explore RNA content of MAEL immunoprecipitates. To this end, we performed RNA-Seq (100 nt long reads) on RNA isolates from two independent MAEL immunoprecipitates (designated A and B). Since the *Mael* mutation has a profound effect on levels of transposon RNAs and alters production of piRNAs (Soper *et al*, 2008; Aravin *et al*, 2009), to control for the non-specific binding of RNPs from wild-type testicular protein lysates, we sequenced RNA immunoprecipitated using total rabbit IgGs. In addition, to better judge potential enrichment of MAEL-associated RNAs, we sequenced total RNA depleted for rRNA sequences from the same wild-type testicular material used for MAEL and IgG RNA immunoprecipitations (RIP). Initially, we counted sequencing reads mapping in 10-kb windows tiled across the entire mouse genome. This analysis revealed a strong and reproducible enrichment of both MAEL RIPs for reads mapping to pachytene piRNA precursor genes (Fig 2A–D and Supplementary Table S2) (Li *et al*, 2013a). Subsequent counting of sequencing reads mapping to protein coding, retrotransposon, and piRNA precursor transcripts has confirmed the original observation and also identified retrotransposons L1 and IAP transcripts as specifically enriched in MAEL RIP (Fig 2E). In addition to pachytene piRNA precursor transcripts and transposons, an additional 40 known mRNAs as well as transcripts originating from hypothetical protein-coding genes (35), pseudogenes (23), and predicted non-coding RNA loci (12) were significantly enriched in both MAEL RIPs (Supplementary Table S3).

Since piRNA processing from primary piRNA precursors likely necessitates their cleavage into shorter molecules (Vourekas *et al*, 2012; Saxe *et al*, 2013), we asked whether MAEL immunoprecipitates contained intermediates of piRNA processing that fall below the lower size limit of approximately 200 nt of the method for RNA-Seq library construction used by us. We therefore generated and sequenced small RNA libraries from size-selected mid- (50–150 nt) and small-sized (15–50 nt) RNAs from MAEL complexes. Counting sequencing reads from both of these size-selected libraries mapping to various classes of cellular transcripts again revealed enrichment of RNA sequences corresponding to pachytene piRNA primary transcripts and retrotransposons (Fig 2F and G). Therefore, MAEL-associated RNAs of all three sizes (15–50, 50–150 and > 200 nt) were enriched for pachytene piRNA precursors (Fig 2H). To better understand the relationship between RNAs of different sizes, we examined patterns of their mapping to individual primary piRNA transcripts. Interestingly, long, medium, and short RNAs exhibited distinct and discontinuous mapping patterns along individual piRNA genes (Fig 2I). Each pachytene piRNA precursor transcript possessed its unique pattern of mapped reads, but, in general, long fragments of piRNA precursors formed a few prominent peaks while small and mid-sized RNA reads formed numerous peaks throughout the transcript that were frequently underrepresented in areas of accumulation of long RNA fragments. These complex mapping patterns were specific to MAEL complexes and not observed for sequencing reads from total testicular RNA. In addition, mapping patterns of MAEL-associated pachytene piRNA precursor RNA reads did not reproduce the mapping pattern observed for piRNAs sequenced from total testicular material (Fig 2I). This suggested that MAEL-containing complexes are enriched in fragments of pachytene piRNA primary transcripts and are depleted of sequences found in mature piRNAs. The simplest explanation of these results is that MAEL resides in RNPs that include Tudor-domain proteins, Piwi proteins, and pachytene piRNA primary transcripts undergoing processing to piRNAs.

A large population of Mael^{129}-null spermatocytes extinguish L1 expression

We next set out to assess the functional significance of MAEL for pachytene piRNA biogenesis and function. Because of the uniform arrest of spermatogenesis in meiotic prophase I, previously described *Mael*^{B6}-null mice were not suitable for this analysis

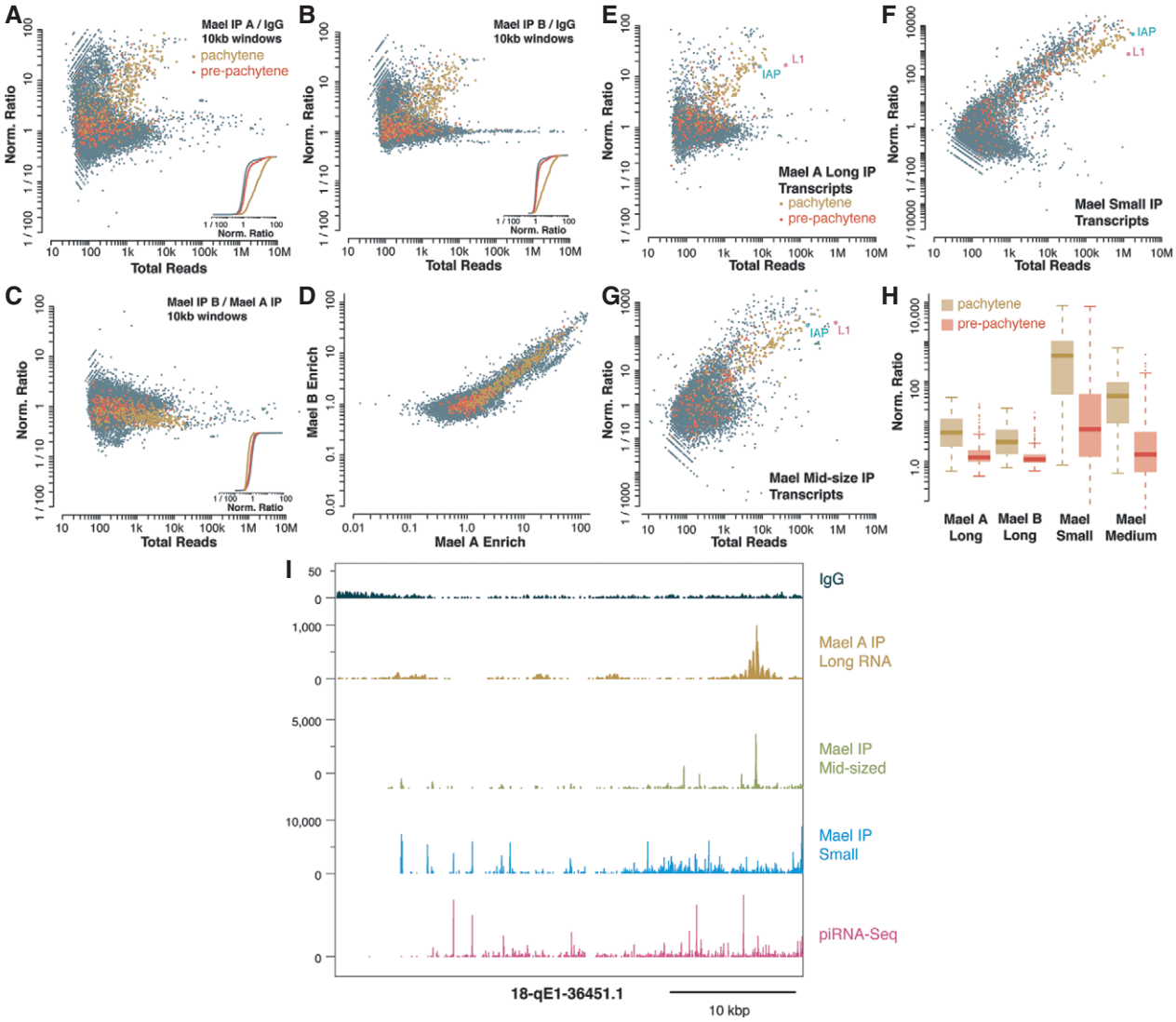

Figure 2. MAEL associates with pachytene piRNA precursors.

A–D Enrichment of piRNA precursors in two independent MAEL immunoprecipitates relative to an IgG control. Sequencing reads in each sample were counted in 10-kb windows tiled across the mouse genome, and samples were compared pairwise by plotting the ratio in read counts, normalized against the median ratio across the genome for each comparison (described further in Materials and Methods), against the total (unnormalized) read count across the two samples. Genomic windows that overlap pachytene piRNA clusters are shown in yellow, and windows that overlap prepachytene piRNA clusters are shown in red; all other windows are plotted in gray. The insets show a cumulative histogram of enrichment ratios for windows with at least 100 total reads, for the genome overall (gray) and for windows overlapping pachytene (yellow) and prepachytene (red) clusters. Comparisons are shown for the first MAEL IP against the IgG control (A), the second MAEL IP against the IgG control (B), and the two MAEL IPs against each other (C). For windows with at least 100 total reads, the enrichment ratios of the two MAEL IPs relative to the IgG control are plotted against each other as well (D).

E–G Enrichment of pachytene piRNA precursor and retrotransposon RNAs in MAEL IP. Sequencing reads aligning to protein-coding, retrotransposon, and piRNA precursor transcripts were counted in each sample. Comparisons of read counts were plotted as above, for total RNA-Seq on MAEL IP (E) as well as size-selected small (F) and mid-sized (G) RNAs. Protein-coding transcripts are shown in gray, while pachytene piRNA clusters are shown in yellow and prepachytene piRNA clusters are shown in red. Retrotransposons are highlighted and labeled individually.

H Enrichment ratios for pachytene and prepachytene piRNA precursor transcripts with at least 100 total reads are summarized in a box-and-whisker plot.

I Differential mapping patterns of long, mid-sized, and small RNAs originating from 18-qE1-36451.1 pachytene piRNA gene immunoprecipitated with MAEL or control antibodies. Lower panel shows piRNA reads from total adult testis mapping to the precursor gene.

(Soper *et al*, 2008). We overcame this limitation by focusing on phenotypes of *Mael*-null mutants backcrossed for over 10 generations to the 129SvJae (129) strain of mice. In contrast to B6 mice, we observed two patterns of L1ORF1p staining within seminiferous tubules in $Mael^{129}$-null animals: a B6-like pattern, containing groups of spermatocytes with high nuclear levels of L1ORF1p (Fig 3B, arrowheads), and a wild-type pattern where cytoplasmic L1ORF1p signal is present in early meiotic prophase I spermatocytes but is extinguished by pachynema (Fig 3C). $Mael^{129}$-null spermatocytes with high levels of nuclear L1ORF1p also show elevated γH2AX nuclear levels (Fig 3B, arrowheads), while γH2AX signal appears normal in $Mael^{129}$-null tubules with a wild-type L1ORF1p staining

pattern (Fig 3C, arrowheads highlight the sex body). To estimate the percent of *Mael*^{129}-null spermatocytes eliminated at the mid-pachytene checkpoint, we immunostained nuclear spreads of WT and *Mael*^{129}-null spermatocytes with antibodies to histone H1t that becomes incorporated into meiotic chromatin of mid-pachytene spermatocytes (Fig 3D) (Moens, 1995; van der Heijden *et al*, 2007). We determined the ratio of mid-to-late (H1t^{+}) to early (H1t^{-}) WT pachytene spermatocytes being 1.4 (Fig 1F). In contrast, the ratio of mid-to-late (H1t^{+}) to early (H1t^{-}) *Mael*^{129}-null pachytene spermatocytes was 0.89 which indicated the failure of a subpopulation of *Mael*-mutant spermatocytes to progress past the mid-point of pachynema. Since the *Mael* mutation did not alter the rate of meiotic prophase I progression [as indicated by the presence of canonical germ cell associations known as stages (Fig 4B and C) (Russell *et al*, 1990)], we estimated that approximately 36.6% [(53 (47%/1.4))/53] of early pachytene *Mael*^{129}-null spermatocytes have been eliminated at the mid-pachytene checkpoint. Therefore, 63.4% of *Mael*^{129}-mutant spermatocytes are capable of silencing L1 expression and do not accumulate meiotic defects that trigger mid-pachytene apoptosis.

Two additional points of spermatogenic failure in Mael^{129}-null mutants

Despite L1 silencing in a large population of mutant spermatocytes, *Mael*^{129}-null males had smaller testes (although larger than that of *Mael*$^{B6-/-}$ mutants) (Supplementary Fig S4) and remained infertile. In light of previously reported abundant expression of MAEL in mid-pachytene spermatocytes, during meiotic divisions and in haploid round spermatids, this observation suggested an additional essential function of MAEL in spermatogenesis (Soper *et al*, 2008). Histological analysis of testes of adult *Mael*^{129}-null mutants using hematoxylin and eosin stain (H&E) revealed an additional wave of degenerating spermatocytes in stage XII seminiferous tubules with cells undergoing meiotic divisions (Fig 4A–C). Since the presence of chromosomal univalents triggers checkpoint leading to spermatocyte death during meiotic divisions, we studied the frequency of such a defect in wild-type and *Mael*^{129}-mutant testes (Eaker *et al*, 2002). We observed univalent chromosomes in 63% of *Mael*^{129}-null MI spermatocytes compared to 29% in the heterozygote (Fig 4D–F). Therefore, 37% of MI *Mael*^{129}-null spermatocytes (or 24% of the starting *Mael*-mutant spermatocyte population) are expected to reach spermiogenesis.

To assess the extent of spermiogenesis in *Mael*^{129}-null testes, we used the periodic acid–Schiff (PAS) stain to reveal the carbohydrate-rich acrosome, a cap-like secretory vesicle attached to the nucleus that gradually forms throughout spermiogenesis (Leblond & Clermont, 1952; Clermont & Perey, 1957; Russell *et al*, 1990). In contrast to characteristic enlargement and spreading of the acrosome over the nuclear surface in the wild-type spermatids, we observed only small PAS-stained organelles in *Mael*^{129}-null round spermatids consistent with an early defect in acrosome formation (Fig 5A and B). Similarly, immunofluorescence analysis of the first cohort of round spermatids in wild-type and *Mael*$^{129-/-}$ P22 testes using mSP-10 antibody showed a single acrosome granule in wild-type early round spermatids but mostly diffuse cytoplasmic staining in *Mael*^{129}-null round spermatids (Fig 5C and D) (Reddi *et al*, 1995). To reveal defects in acrosome formation in further details, we examined wild-type and *Mael*^{129}-null round spermatids by electron microscopy and observed the presence of the proacrosomal vesicle but lack of further maturation of the acrosome (Fig 5E and F). Taken together with the results of PAS staining and immunofluorescence analysis, these observations indicated steps 1–2 arrest of spermiogenesis in the absence of MAEL. Despite lacking the acrosome, mutant round spermatids went on to develop a thickened nuclear lamina that normally underlies the expanding acrosomal sack (Fig 5E and F) (Russell *et al*, 1990). Notably, the extent of nuclear lamina spreading observed in *Mael*^{129}-mutant round spermatids was comparable to that of step 7 wild-type round spermatids (Fig 5E and F). This observation suggested that acrosome-deficient round spermatids might persist in the *Mael*^{129}-mutant testes until step 7 of spermiogenesis.

Another prominent structure with a stereotypical timeline of formation in the developing round spermatid is the flagellum. In the wild-type mouse, flagellum formation is initiated by two centrioles forming an axoneme with a "9 + 2" arrangement of microtubules in step 6 round spermatids (Russell *et al*, 1990). EM analysis and staining for acetylated tubulin revealed the presence of disorganized flagella in the early phase of maturation in *Mael*^{129}-null testis (Fig 5G–L).

Since MAEL, MIWI, and Tudor-domain protein are known to localize to the chromatoid body of round spermatids and required for its integrity, we asked whether the spermiogenic arrest of the *Mael*^{129} mutant could be attributed to defects in chromatoid body structure or localization of these proteins. EM and immunofluorescence studies did not identify any appreciable differences in the appearance of chromatoid bodies in EM images and localization of MIWI, MVH, TDRD1, and TDRD6 in *Mael*^{129}-null round spermatids (Supplementary Fig S5).

As we have shown earlier, 63% of *Mael*^{129}-null spermatocytes capable of silencing L1 in meiotic prophase I nonetheless failed to establish functional crossovers resulting in their elimination during meiotic divisions. This observation also raised a possibility that nuclei of *Mael*^{129}-null round spermatids might also be deficient in

Figure 3. Some *Mael*^{129}-null spermatocytes silence L1.

A Immunofluorescence image showing cytoplasmic L1 ORF1p (green) and γH2AX phosphorylation (magenta) in P21 *Mael*$^{129+/-}$ spermatocytes. γH2AX "patch" (arrowheads) marks the sex body of pachytene spermatocytes (scale bar, 20 μm; white = DAPI).

B Immunofluorescence image showing cytoplasmic and nuclear ORF1p (green) and γH2AX (magenta) in P21 *Mael*$^{129-/-}$ spermatocytes. Arrowheads highlight pachytene spermatocytes with nuclear ORF1p and massive accumulation of γH2AX signal (scale bar, 20 μm; white = DAPI).

C Immunofluorescence image showing cytoplasmic ORF1p (green) and γH2AX (magenta) in P21 *Mael*$^{129-/-}$ spermatocytes in a stage X tubule. Arrowheads highlight pachytene spermatocytes with no cytoplasmic or nuclear ORF1p signal and containing γH2AX-positive sex bodies (scale bar, 20 μm; white = DAPI).

D An example of an immunofluorescence nuclear spread of a wild-type early pachytene spermatocyte lacking histone H1t in the meiotic chromatin. Shown are individual channels for histone H1t and SYCP3, and the merged image. SYCP3 was used to identify pachytene spermatocytes to be scored for H1t expression.

E An example of a mid-to-late (H1t^{+}) wild-type spermatocyte exhibiting histone H1t incorporation in the meiotic chromatin.

F Quantification of early (H1t^{-}) and mid-to-late (H1t^{+}) spermatocytes in testes of wild-type and *Mael*$^{129-/-}$ animals.

some aspect of genome structure or function. In fact, we did observe that a minor population of round spermatids were positive for γH2AX. Since we did not detect L1ORF1p in *Mael*^{129}-null round spermatids, we attribute that signal to apoptosis (Supplementary Fig S6). To assess the developmental potential of the nuclei of arrested *Mael*^{129}-null round spermatids, we performed round spermatid nuclear injection (ROSNI) into wild-type MII oocytes (Ogura *et al*, 1994; Yanagimachi *et al*, 2004). With ROSNI, we were able to generate six pups (Fig 5M) four of which developed into fertile adults (Fig 5N). Since the efficiency of ROSNI using *Mael*^{129}-null round

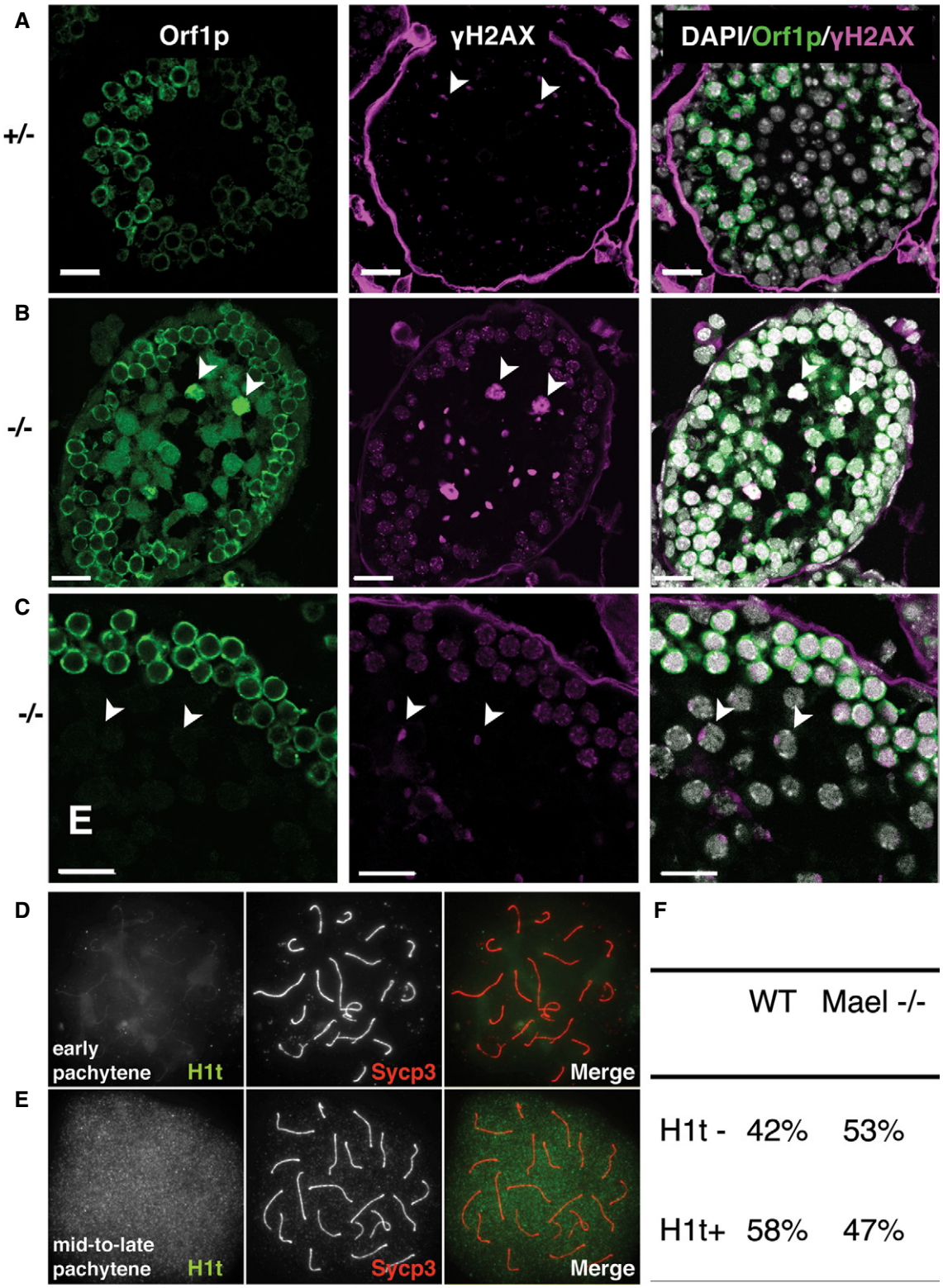

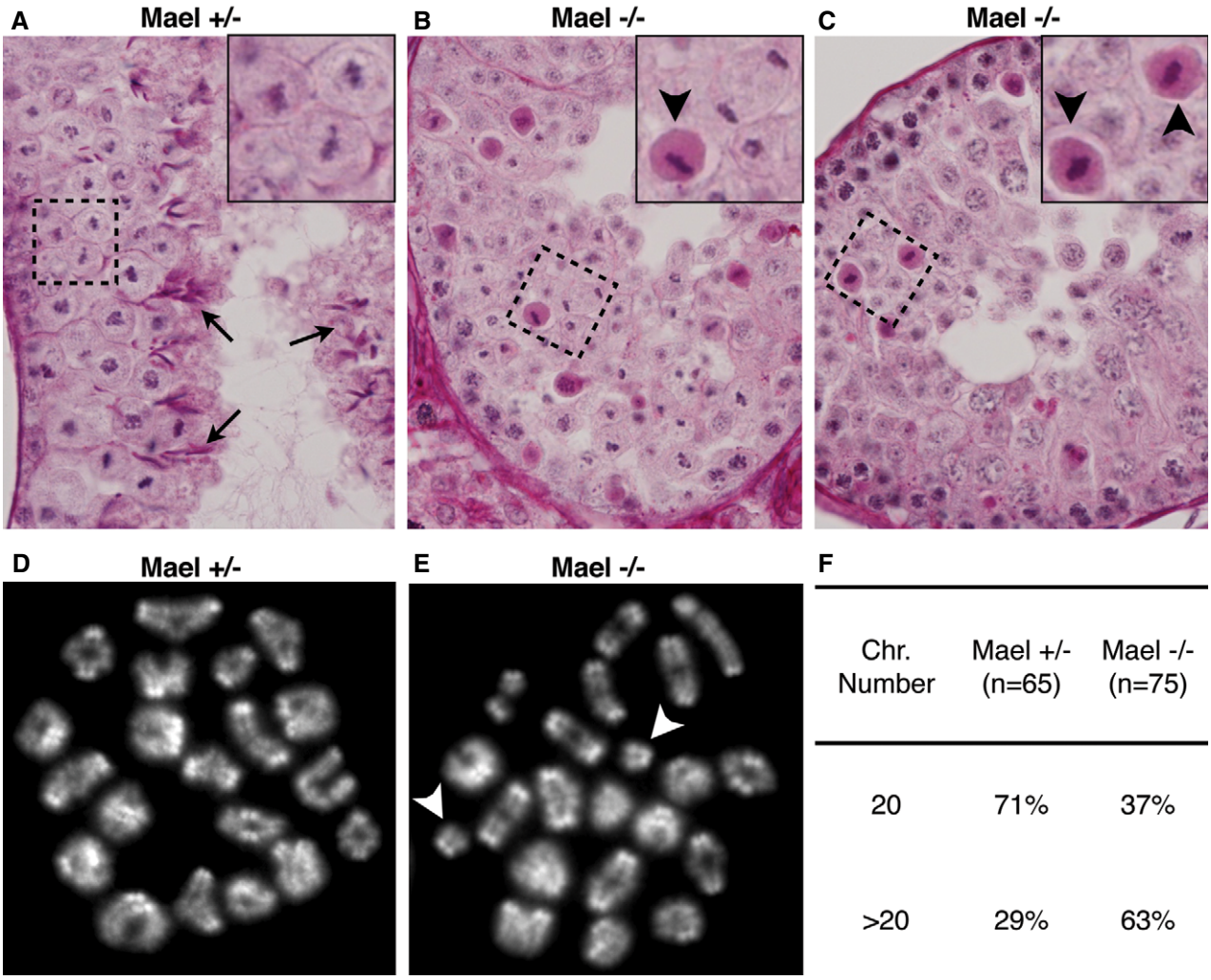

Figure 4. Meiotic metaphase I/II arrest of *Mael*$^{129-/-}$ spermatocytes.

A H&E-stained section showing a segment of wild-type stage XII seminiferous tubule. Arrows indicate elongate spermatids.

B, C H&E-stained section of *Mael*$^{129-/-}$ testis showing a stage XII tubule with apoptotic mutant spermatocytes (arrowheads). Note that *Mael*^{129}-mutant tubules lack step 12 spermatids seen in the WT (arrows) (A).

D–F Metaphase I spreads of wild-type (D) and *Mael*^{129}-null (E) spermatocytes and quantification (F) of the data. Arrowheads in (E) indicate univalent chromosomes.

spermatids compared favorably to prior experiments of others using wild-type round spermatids (Fig 5O), we conclude that at least 20% of round spermatid nuclei are developmentally competent or at least do not harbor irreparable damage to the genome (Ogura *et al*, 1994; Yanagimachi *et al*, 2004; Yabuta *et al*, 2011).

Taken together, these results suggest that a subpopulation of *Mael*^{129}-null spermatocytes are capable of repressing L1 to the extent that allows them to progress to the post-meiotic stage of germ cell differentiation. However, even in the absence of obvious signs of L1 activation and with a developmentally competent genome, *Mael*^{129}-deficient round spermatids fail to undergo normal spermiogenesis.

Mael is required for piRNA production

To investigate the requirement for MAEL in the production of piRNAs, we preformed two independent sequencing runs of size-selected 18–35 nt RNAs from testes of wild-type and *Mael*^{129}-null animals. To reduce the potential impact of arrested and degenerating round spermatids on the overall picture of piRNA production in the *Mael*^{129} mutant, we used testes of 21-day-old animals that contain early-stage round spermatids. Sequencing of small RNAs from wild-type testes generated a characteristic profile with 21–22, 26–27, and 30 nt peaks that corresponded to miRNAs, MILI-, and MIWI-bound piRNAs, respectively (Fig 6A). In contrast to the wild-type, piRNA levels of *Mael*^{129}-mutant testes were tenfold lower when normalized to miRNAs (Fig 6A and Supplementary Fig S7). In agreement with results of MAEL RIP experiments, pachytene non-coding piRNAs were specifically affected compared to pre-pachytene piRNAs (Fig 6B and C, and Supplementary Fig S8). In addition, we observed an increase in the production of piRNAs from exonic sequences of mRNAs, principally those containing defined prepachytene piRNA precursors (Li *et al*, 2013a) (Fig 6D). These results suggest that MAEL is required for the efficient production of piRNAs specifically from non-coding pachytene piRNA precursor transcripts.

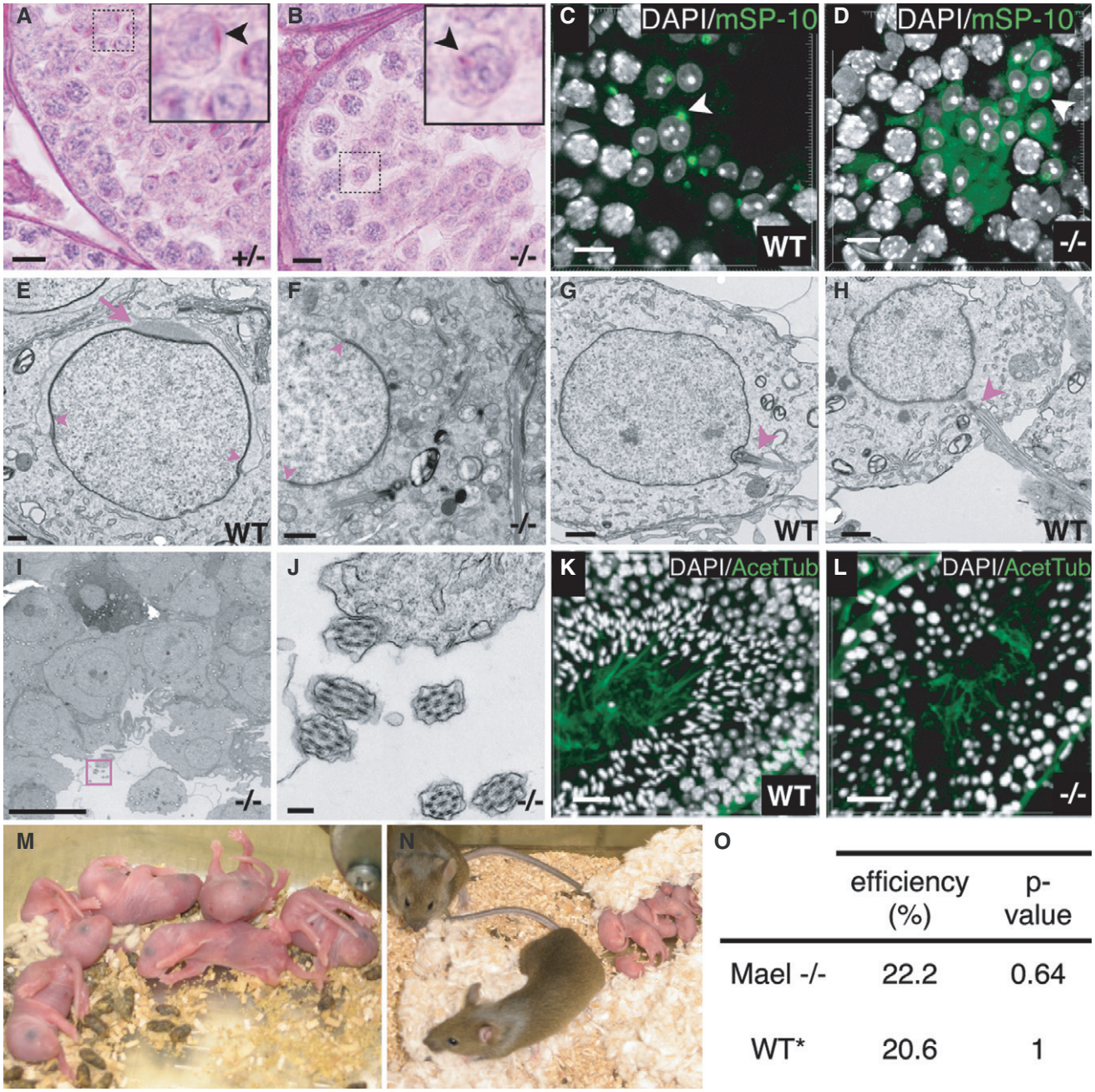

Figure 5. Spermiogenic arrest of *Mael*^{129}-null germ cells.

A PAS staining of a Mael$^{+/-}$ Stage V seminiferous tubule. Inset shows a close-up image of round spermatids with a PAS-stained acrosome cap. Arrowhead highlights a developing acrosome cap in step 5 round spermatids (scale bar, 10 μm).

B A PAS-stained Stage V seminiferous tubule of *Mael*$^{129-/-}$ testis showing reduced size of PAS-stained acrosomes in the mutant. Inset shows a mutant round spermatid with a small dot of PAS-stained material (arrowhead) (scale bar, 10 μm).

C, D Projections of a Z-stack of immunofluorescence of proacrosomal vesicles visualized with antibodies to mSP-10 (green, arrowheads) in wild-type P22 (C) and *Mael*$^{129-/-}$ (D) round spermatids. (white, DAPI; scale bars, 10 μm).

E EM of a WT step 7 round spermatid showing developing acrosome (arrow), a nuclear dense lamina and marginal fossa (arrowheads) (scale bar, 0.5 μm).

F EM image of *Mael*^{129}-null spermatid with nuclear dense lamina (arrowheads) but lacking the acrosome and marginal fossa (scale bar, 0.5 μm).

G, H EM of WT step 7 round spermatids with tails (arrowheads) impacting the nucleus. (scale bars, 1 μm).

I, J Several *Mael*^{129}-null spermatids (I: scale bar, 10 μm) and bundle of flagella (boxed) showing "9 + 2" arrangement of microtubules (J: scale bar, 0.5 μm).

K, L Projections of a z-stack of immunofluorescence of stage VI wild-type (K) and *Mael*^{129}-null (L) tubules stained with anti-acetylated tubulin antibody (green) (white, DAPI; scale bars, 30 μm).

M Live progeny produced from wild-type oocytes injected with nuclei of *Mael*^{129}-null round spermatids.

N Adult mice produced by ROSNI and their viable progeny.

O Efficiency of ROSNI using *Mael*^{129}-null round spermatids is comparable to the wild type [*—data from Yanagimachi *et al* (2004)].

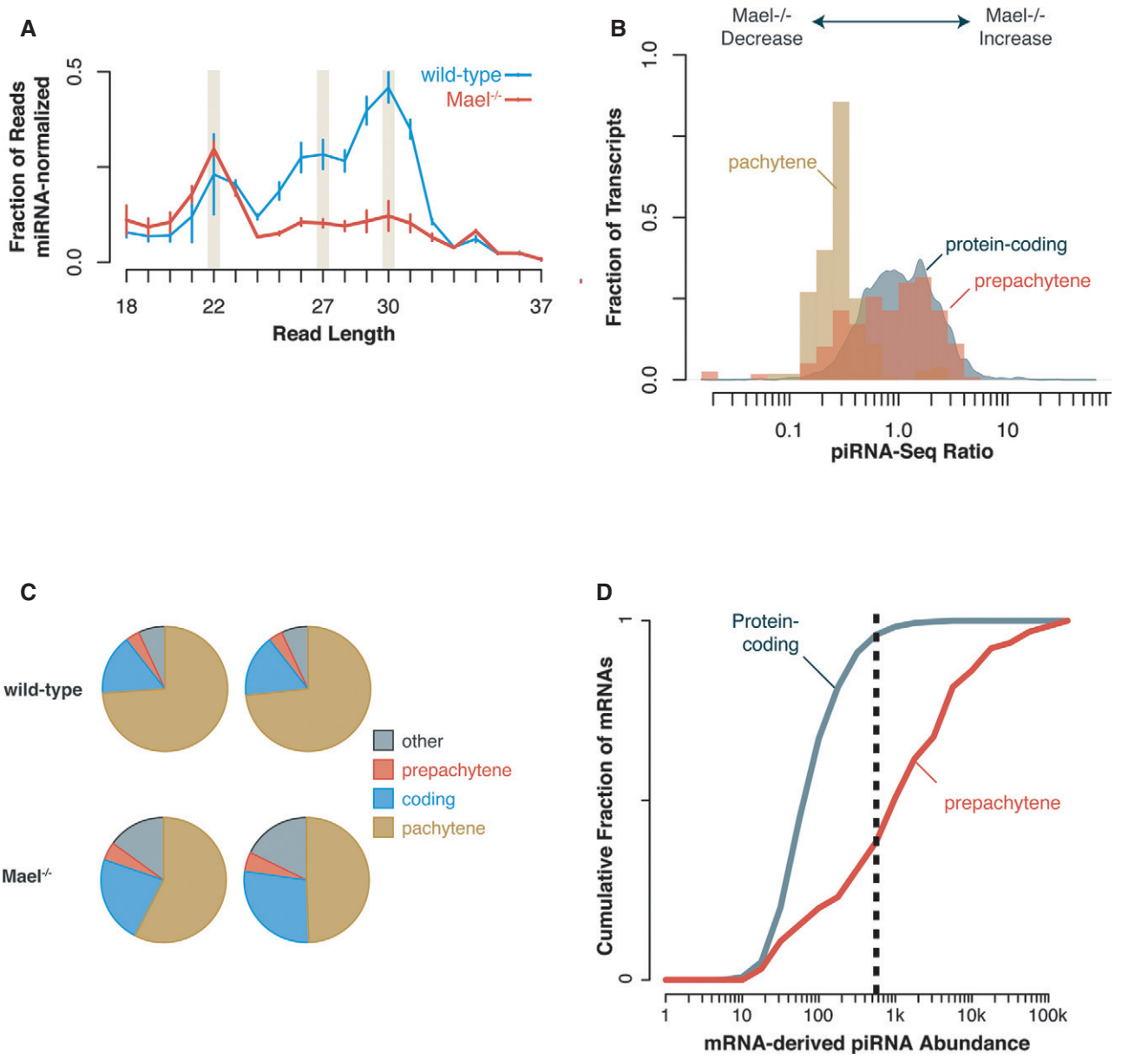

Figure 6. MAEL is required for pachytene piRNA biogenesis.

A Small RNA length distributions from WT and *Mael*^{129}-null P21 testes. The lengths of all small RNA sequencing reads in two biological replicates of each genotype were tabulated to produce length distributions. The average and standard deviation of these length distributions was calculated for each genotype, and these values were then scaled by the fraction of miRNA-sized fragments (19–25 nt) and plotted.

B Specific reduction of pachytene piRNAs in *Mael*^{129}-null P21 testis. The number of piRNA-sized (26–32 nt) small RNA alignments was counted for each transcript in two biological replicates of each genotype. These raw counts were normalized to account for differences in read depth between samples, and the effect of *Mael*^{129}-null genotype, relative to wild-type, on the number of piRNA reads was calculated for each transcript. A kernel density estimate (protein-coding mRNAs) or a histogram (piRNA precursors) is plotted for each class of transcript.

C Classification of piRNAs in pairs of WT and *Mael*^{129}-null P21 testes. The fraction of piRNA-sized small RNA reads aligning to each class of transcript was counted in two biological replicates of wild-type and *Mael*^{129}-null samples.

D Abundance of piRNAs derived from mRNAs defined as prepachytene piRNA precursors compared to all other mRNAs present in testes. Transcripts present at reasonable abundance (> 100 reads) in mRNA-Seq analysis were classified based on their overlap with annotated piRNA precursors. The piRNA abundance in wild-type P21 testes was calculated from the number of reads obtained in two biological replicate small RNA sequencing samples.

Reduced translation of spermiogenic mRNAs in the *Mael*^{129} mutant

To further understand the origin of spermiogenic phenotypes in the *Mael* mutant, we performed RNA-seq analysis in parallel with ribosome profiling in testes of P21 wild-type and *Mael*^{129}-null animals. The method of genome-wide ribosome profiling utilizes the power of deep sequencing to accurately monitor mRNA translation and to obtain insights into the regulation and mechanism of protein

translation in animals and plants (Ingolia *et al*, 2009, 2012; Ingolia, 2014). This analysis allowed us to determine expression and translation levels of 7,434 mRNAs and revealed reduced translational efficiency of 880 transcripts in testes of *Mael*^{129}-null mice (Fig 7A and Supplementary Table S4). To verify translational repression of candidate mRNAs in the *Mael*^{129} mutant, we performed semi-quantitative RT–PCR on sucrose gradient fractions obtained from wild-type and *Mael*^{129}-null testes (as described below). In agreement with ribosome profiling data, this analysis confirmed translational repression in the *Mael*^{129} mutant and revealed reduced levels of testicular mRNAs in translationally most active fractions of the gradient with corresponding increase in fractions with lower ribosome occupancy (Supplementary Fig S9). Strikingly, Gene Ontology analysis of transcripts with decreased translational efficiency in the *Mael*^{129} mutant identified many as involved in acrosome and flagellum formation (Gene Ontology data: Supplementary Fig S10 and Supplementary Table S5) (Zheng & Wang, 2008).

We investigated more broadly the correlations between piRNA, mRNA, and translational changes in *Mael*^{129}-null testes. Genes whose translation was reduced in *Mael*^{129}-null testes also showed decreased piRNA levels (Fig 7B), and in fact, we found stronger positive correlation between changes in mRNA and piRNA levels (Fig 7C). These data suggest that mRNA-derived piRNAs produced in the absence of MAEL reflect the overall composition of the transcriptome and that the additional piRNAs do not greatly impact the stability and translation of precursor mRNAs, nor does their production dramatically deplete precursor transcripts. Finally, we asked whether the *Mael* mutation affects translation of mRNAs predicted to be bound and stabilized and translationally repressed by MIWI (Vourekas *et al*, 2012). This analysis revealed that while there is a modest enrichment for such mRNAs, most mRNAs translationally downregulated in the *Mael* mutant come from the pool of normally expressed transcripts (Supplementary Fig S11). The combination of these results with apparent lack of excessive DNA damage and L1 overexpression in *Mael*^{129}-null round spermatids and whose genomes are capable of supporting development following ROSNI suggest that translational defects underlie spermiogenic arrest in the absence of MAEL.

Given prior evidence of MIWI association with the translational machinery (Grivna *et al*, 2006b), we asked whether MAEL (and perhaps piRNA precursors) contributes to translation of spermiogenic mRNAs through its association with polysomes. To this end, we used velocity sedimentation of a testis lysate through a 10–50% sucrose gradient that we validated by revealing the expected pattern of 80S ribosome and polysome distribution based on A_{260} values, distribution of 40S ribosomal protein S6 (RPS6) and rRNA (Fig 8A). Furthermore, we used antibodies to dynein intermediate chain (DIC) to identify the position the approximately 20S (1–2 MDa) dynein motor complex within the gradient (Bingham *et al*, 1998; King *et al*, 2002). We first corroborated a previously reported distribution of MIWI across the gradient including in polysome fractions. Under these experimental conditions, a majority of MAEL protein was observed in the top four fractions overlapping DIC-containing fractions 2–4 in the 4.5–20S range with the remaining protein trailing deep in the gradient into the polysome fractions (Fig 8A). Centrifugation of testicular protein lysates in the presence of EDTA, which disrupts both polysomes and RNPs (Spirin, 1974; Newton *et al*, 1975), resulted in the loss of MIWI from polysome-containing fractions similar to RPS6 (Fig 8B). EDTA treatment also altered sedimentation of MAEL albeit to a lesser extent than what was observed for MIWI. To better differentiate polysome versus RNP association of MAEL, we centrifuged testicular lysates in the presence of puromycin (Blobel & Sabatini, 1971). This has profoundly changed the sedimentation profile of RPS6 but had only a modest effect on MIWI and MAEL (Fig 8C). These results suggested that MIWI and MAEL might reside in EDTA-sensitive RNPs of variable density which allows for their broad distribution including deep into the gradient. Given our earlier findings of pachytene piRNA precursors co-immunoprecipitating with MAEL, we examined their sedimentation profile in sucrose gradients. The sedimentation profile of MAEL-associated fragments of piRNA precursor transcript from chromosome 6 (assessed by three independent RT–PCR amplicons) was strongly altered by EDTA but minimally by puromycin treatment (Fig 8B and C) further supporting their RNP nature. Consistent with this observation, we did not observe enrichment of piRNA precursor fragments in ribosome-protected footprints (Supplementary Fig S12). Taken together, these observations suggest that while a minority of MAEL sediments with polysomes in sucrose gradients, its behavior is consistent with it being assembled in RNPs rather than associating with the translational machinery.

Discussion

A central aim of this study was to obtain new insights into the piRNA pathway in adult mouse testis. We approached this problem by studying a conserved protein MAEL that is essential for transposon control in meiotic prophase I (Soper *et al*, 2008). We immunopurified MAEL complexes from adult testicular lysates and determined that they contained, among others, MIWI, several Tudor-domain proteins and pachytene piRNA precursors. These findings raised a possibility that MAEL functions in post-meiotic, haploid round spermatids, which was consistent with expression of MAEL in round and elongate spermatids (Soper *et al*, 2008). Since previously reported *Mael*-mutant mice in the B6 genetic background undergo mid-meiotic prophase I spermatogenic arrest, we asked whether *Mael* spermatogenic phenotype could be modified by backcrossing to the 129SvJae strain. This analysis revealed two additional points of spermatogenic arrest including during meiotic divisions and, most importantly, in round spermatids with prominent defects in acrosome and flagellum formation. At the same time, nuclei of at least 20% of *Mael*^{129}-null round spermatids were compatible with development following the ROSNI procedure. Further molecular analysis of the *Mael*^{129} mutant revealed that abrogation of MAEL function results in a severe reduction of pachytene piRNA levels and diminished translation of spermiogenic mRNAs including those coding for acrosomal and sperm tail proteins. Finally, MAEL and pachytene piRNA precursor sedimentation in sucrose gradients is consistent with a ribonucleoprotein nature of their complexes rather than with translational apparatus.

In contrast to results of MS analysis of MAEL-associated proteins in the fly ovary (Sato *et al*, 2011), we identified several piRNA pathway proteins in immunopurified MAEL complexes proteins including MIWI and Tudor-domain proteins. This result is consistent with prior identification of MAEL as a component of MIWI- and MILI-associated proteomes (Vagin *et al*, 2009). We were able to confirm

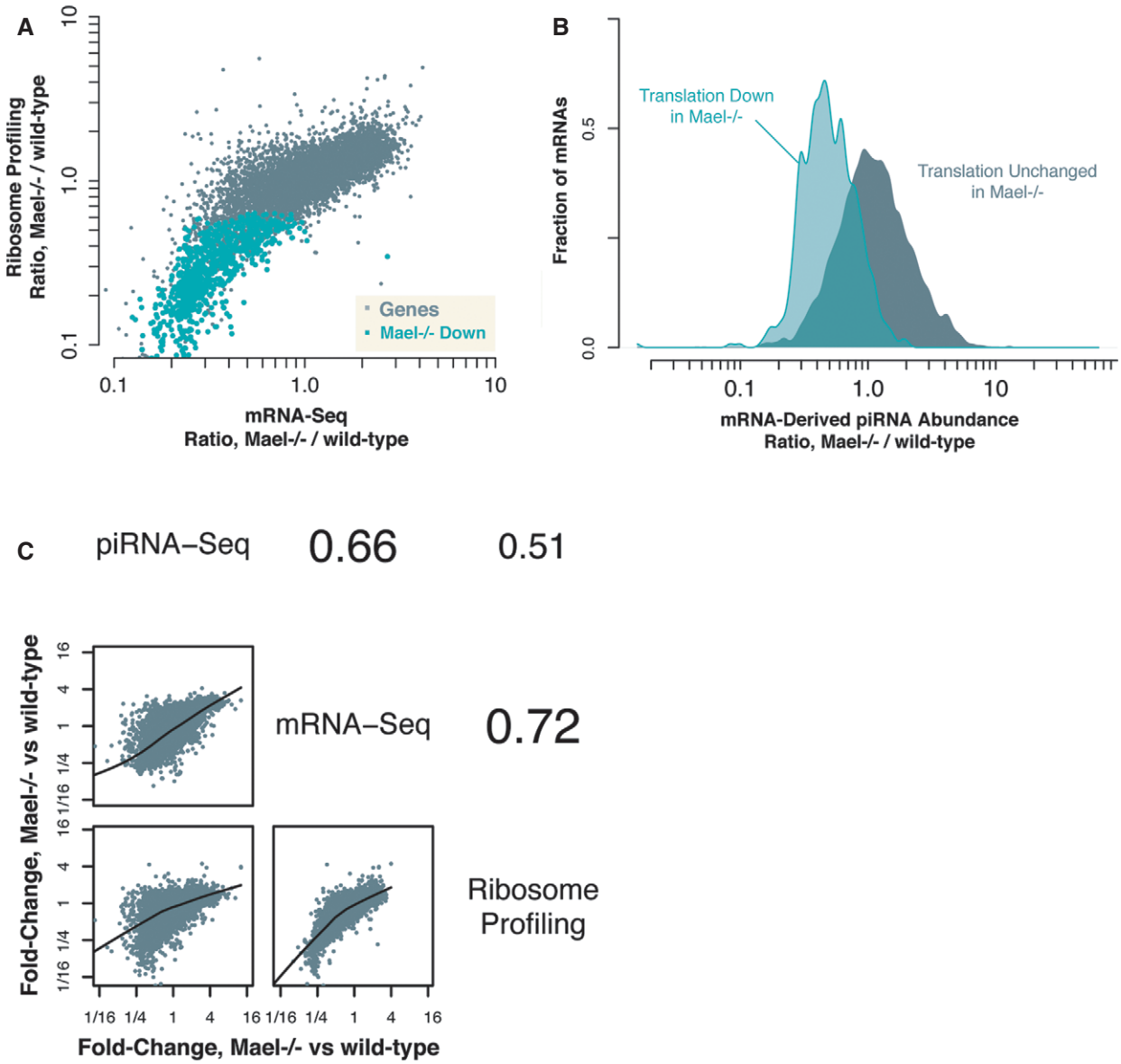

Figure 7. Translation of spermiogenic mRNAs is abrogated in the *Mael*^{129} mutant.

A Scatter plot showing mRNA level changes (*x*-axis) against ribosome profiling changes (*y*-axis) between *Mael*^{129}-null and wild-type testes.

B Reduced translation of mRNAs is not due to their consumption by the piRNA machinery. The fold change in the abundance of piRNAs mapping to protein-coding mRNAs between *Mael*^{129}-null and wild-type testes was computed for all mRNAs. Kernel density estimates of these fold changes are plotted for transcripts that showed reduced translation in *Mael*^{129}-null, as assessed by ribosome profiling, and for transcripts that did not show reduced translation.

C Correlation analysis of mRNA-derived piRNA production with levels of mRNA expression and translation. The *Mael*^{129}-null and wild-type fold change in piRNAs, mRNA-seq abundance, and ribosome-protected footprints is compared pairwise for each protein-coding transcript. Individual genes and a LOESS regression fit are plotted on the lower left-hand part of the matrix. The Pearson correlation of the log fold-change values is shown on the upper right-hand part of the matrix.

MAEL–MIWI co-immunoprecipitation by Western blot analysis from adult testicular lysates and in a heterologous system of HEK293T-cultured cells. Similarly, we validated MAEL–TDRD6 interactions in testicular and cultured cell protein lysates. Importantly, both sets of interactions were unaffected by the addition of RNase A, thus arguing against an RNA-mediated bridging of proteins. The fact that MAEL immunoprecipitated TDRD6 from HEK293T cell lysate, which likely lacked other components of the piRNA pathway, provides a strong indication that these proteins interact directly. In contrast to sDMA-mediated interaction of Piwi proteins, including MIWI and MILI, with Tudor-domain proteins, we did not detect the arginine methylation on MAEL which suggests that MAEL interacts with TDRD6 in a manner distinct from that of Piwi proteins raising a possibility of MIWI and MAEL binding to same TDRD6 scaffold protein. Unlike for MIWI, we did not observe MILI co-immunoprecipitation with MAEL on Western blots. Given distinct sensitivities of MS versus antibody-based detection, we cannot rule out that MILI still interacts with MAEL directly or whether this interaction is

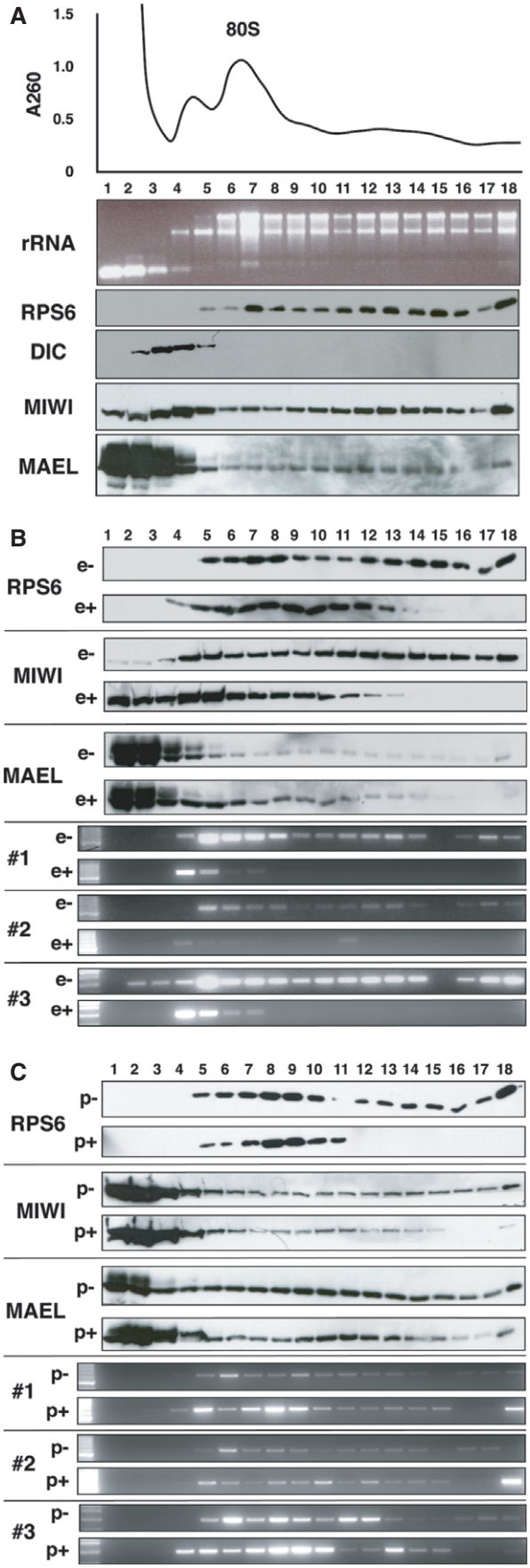

Figure 8. Velocity sedimentation analysis of MAEL-pachytene piRNA precursor complexes.

A Sucrose density gradient sedimentation profiles of MAEL and MIWI in native protein lysates from adult WT mouse testes. Dynein intermediate chain (DIC), ribosomal RPS6 protein, and rRNA sedimentation profiles were used to verify sucrose gradient performance.

B, C Sucrose gradients of testicular protein lysates with and without pretreatment with puromycin (p+, p−) (B) or EDTA (e−, e+) (C). Effects of puromycin and EDTA on sedimentation of a piRNA precursor (Chr. 6) were determined using three RT–PCR amplicons (#1–3) corresponding to MAEL-enriched long RNA fragments.

Source data are available online for this figure.

indirect via a Tudor-domain or other proteins. Likewise, while we were able to corroborate the MS finding of MAEL interaction with RNF17 on Western blots, we did not reproduce this interaction in HEK293T cell protein lysates. Overall, MS analysis of MAEL immunopurified complexes provided important new information on potential interactions of MAEL with proteins in various pathways in adult male germ cells.

Of particular interest is the identification of pachytene piRNA precursors in MAEL-containing complexes. The mechanism of primary piRNA processing is still being elucidated, and the identification of MAEL-containing piRNPs offers a promising approach to expand our understanding of the mechanism governing selective targeting of piRNA primary precursors to sites of subsequent processing into pachytene piRNAs. The simplest explanation for the lack of prepachytene piRNA precursor transcripts in MAEL complexes is their earlier stage of expression, before Myb-A driven upregulation of pachytene piRNA primary transcript and *Mael* expression (Li *et al*, 2013a). RNA-Seq-based identification of long and size-selected short, and small fragments of pachytene piRNA primary transcripts in MAEL complexes suggests that these complexes function as sites of processing of piRNA precursors into mature piRNA. Mapping patterns of reads of different lengths and their divergence from mapping patterns of mature piRNAs suggest that piRNA precursor transcripts (intact or fragmented into large segments) are incorporated into MAEL-containing piRNPs in a manner that results in their asymmetric processing into piRNAs. Reproducible retention of the same long RNA fragments in MAEL complexes could be a product of protecting these sequences from cleavage by RNA folding, interaction with RNA-binding proteins, or preferential utilization of other sequences, depleted from MAEL complexes, for piRNA production. Interestingly, the idea of piRNA precursor fragmentation and processing is consistent with prior immunoelectron microscopy analysis of MAEL localization in spermatocytes and round spermatids where we have consistently observed large nuclear and cytoplasmic MAEL complexes (labeled by 10–15 gold particles) and smaller MAEL complexes (labeled with 1–3 gold particles) localized to electron-dense areas of chromatoid and piP-bodies [Fig 1 and Supplementary Fig S1 in Soper *et al* (2008)]. These observations also imply that individual pachytene piRNA precursor transcripts might interact with several MAEL complexes during their transport to cytoplasmic RNA processing centers. The idea of processing of long piRNA precursor transcripts in MAEL complexes is also supported by results of our velocity centrifugation analysis that revealed RNP rather than polysome-associated behavior of MAEL, MIWI, and piRNA precursors. Whether this association is mediated by a direct interaction of

MAEL with piRNA precursors remains to be elucidated, but the presence of amino-terminal HMG-like box domain and a Maelstrom-specific domain that is computationally predicted to be an RNase H-like fold in MAEL (Zhang *et al*, 2008) does not rule the possibility of interaction and/or cleavage of piRNA transcripts by MAEL.

To demonstrate functional significance of MAEL and MAEL-containing complexes in haploid round spermatids, we have overcome the key limitation of the previously characterized *Mael*-mutant mice bred onto the B6 genetic background by turning to the 129 strain of mice. It is well recognized that genetic background can influence numerous aspects of mouse development and adult physiology including germ cells in the wild-type and transgenic lines (Sanford *et al*, 2001; Doetschman, 2009; Vranis *et al*, 2010). In the specific case of the *Mael* mutation, we posit that the origin of phenotypic variation between the two genetic backgrounds might lie in differential *de novo* DNA methylation of transposable elements in *Mael*-null prospermatogonia that go on to give rise to adult spermatogonial stem cell population (Aravin *et al*, 2008; Kuramochi-Miyagawa *et al*, 2008). Another source of variation might arise from differences in transposon endowments between the two strains' genomes or differences in the stringency of transposon silencing or both, which become unmasked at the onset of meiotic initiation leading to elevated L1 expression observed in several piRNA pathway mutants including *Mael* (Akagi *et al*, 2008; Soper *et al*, 2008; van der Heijden & Bortvin, 2009b; Shoji *et al*, 2009; Tanaka *et al*, 2011; Di Giacomo *et al*, 2013). Differential DNA methylation of L1 between spermatogonial stem cells could account for the pattern of L1ORF1p expression observed in seminiferous tubules of $Mael^{129-/-}$ mice resulting in accumulation of DNA damage and apoptosis of 40% of pachytene spermatocytes in contrast to the 100% spermatocyte lethality in the $Mael^{B6}$ mutant. Absence of DNA damage and asynapsis in 60% of $Mael^{129-/-}$ spermatocytes allowed us to uncover two additional points of spermatogenic arrest in the *Mael* mutant. Terminal arrest of spermatogenesis at the round spermatid stage is reminiscent of phenotypes of *Miwi* and *Tdrd6* mutants (Deng & Lin, 2002; Hosokawa *et al*, 2007; Vasileva *et al*, 2009; Reuter *et al*, 2011; Vourekas *et al*, 2012). All three proteins are prominent in the chromatoid body of round spermatids, and inactivating mutations in all three genes result in spermiogenic arrest. However, in contrast to *Miwi* and *Tdrd6* mutants, abrogation of *Mael* has no effect on MIWI, TDRD1, TRDR6, and MVH localization and the appearance of chromatoid body. However, $Mael^{129}$-null round spermatids show a clear defect in acrosome formation and flagellum. These defects could be the cause of spermiogenic arrest as we did not observe elevated expression of L1, accumulating DNA damage and genomes of at least 20% of $Mael^{129}$-null round spermatids are fully developmentally competent.

Consistent with strong enrichment of pachytene piRNA primary transcripts in MAEL complexes, we find that loss of MAEL function leads to a strong reduction of pachytene piRNA levels in the mutant. Interestingly, even though we could not demonstrate MAEL association with MILI by Western blot analysis, small RNA sequencing in the *Mael* mutant uncovered a lack of both MILI and MIWI interacting piRNAs which agrees with results of MS analysis of MAEL complexes. Therefore, MAEL-associated pachytene piRNA precursors are processed by both Piwi proteins. At the same time, we saw an increase in the relative prepachytene piRNA levels in the *Mael* mutant which agrees with results of MAEL RIP analysis and suggests that prepachytene piRNA processing does not absolutely depend on MAEL function.

As is also true for prior studies focused on pachytene piRNA biogenesis, altered piRNA levels did not provide a straightforward explanation to the molecular basis of spermatogenic arrest in the $Mael^{129}$ mutant. However, genome-wide parallel RNA-Seq and ribosome footprinting analysis revealed that the *Mael* mutation leads to reduced translation of spermiogenic mRNAs many of which encode acrosomal and flagellum proteins and most of which, although not unexpectedly, do not represent MIWI-repressed mRNAs (Vourekas *et al*, 2012). As MAEL is unlikely to be directly regulating translation and its sedimentation behavior on sucrose gradients is consistent with its piRNP identity than polysome association, a different mechanism must be involved in this translational phenomenon. One such potential mechanism could be illegitimate and extensive consumption of spermatogenic mRNAs by piRNA machinery in the absence of MAEL. Yet our analysis did not reveal a significant increase in piRNA produced from such mRNAs in the $Mael^{129}$ mutant. An alternative idea is that the tenfold reduction in pachytene piRNA levels in the $Mael^{129}$ mutant could lead to accumulation of unloaded, piRNA-free MIWI protein. Since MIWI has been shown to bind spermiogenic mRNAs and stabilize them in translationally inactive mRNPs (Vourekas *et al*, 2012), the excess of unloaded MIWI could erroneously bind to normally translated spermiogenic mRNAs leading to their translational repression and, ultimately, to the arrest of spermiogenesis. In addition, as piRNA binding promotes turnover of MIWI (Zhao *et al*, 2013), lower levels of piRNAs might lead to further increase in the cellular pool of free MIWI protein. An important implication of this model is that despite lacking obvious targets in the spermatid transcriptome, pachytene piRNAs might have an important function in mRNA translation as regulators of the availability of MIWI. This idea makes several intriguing predictions that will be tested in future studies.

Materials and Methods

Animals and tissue samples

Construction of $Mael^{B6}$-mutant mice was described previously (Soper *et al*, 2008). 129SvJae mice were obtained from Rudolf Jaenisch (Whitehead Institute, Cambridge, MA). Testes from postnatal day 22 (P22) or adult (3–5 month old) $Mael^{129+/+}$ (wild-type), $Mael^{129+/-}$, and $Mael^{129-/-}$ mice were dissected, the tunica albuginea was removed, and the testes were cut in half transversely prior to fixation. All animal experiments and procedures were approved by IACUC.

Testes for IF were fixed in freshly prepared 2% PFA/1× PBS for 2–3 h on ice, briefly washed with 1× PBS, and incubated in 30% sucrose/1× PBS at 4°C for 12 h and longer. Testes were embedded in OCT blocks, frozen on dry ice, and cryosectioned at 8 μm thickness.

Testes processed for histology were fixed with Bouin's fixative (Sigma) and incubated overnight at 4°C with gentle mixing then washed and stored in 70% ethanol. Paraffin embedding was done

using a Leica TP1020 tissue processor and Leica's EG1160 embedding station. Paraffin sections of testes were cut at 10 μm thickness.

Immunofluorescence

The slides were dried at 42°C for 15 min, washed in 0.1% Triton X-100/PBS, blocked for 30 min at room temperature with primary blocking solution (PBS, 0.1% Triton X-100, 10% normal donkey serum, 3% BSA, and 0.02% azide). Primary antibodies were diluted with primary blocking solution, applied to slides in a humidified chamber, and incubated overnight at 4°C. Slides were then washed with PBS for 10 min and blocked with secondary blocking solution (PBS, 10% normal donkey serum, and 3% BSA) for 30 min at room temperature. Secondary antibodies were diluted with secondary blocking solution, applied to slides, and incubated in a humidified chamber for 2 h at room temperature. The slides were then washed for 5 min in PBS and counterstained with DAPI. Slides were then washed for 5 min in PBS. One quick water wash was performed prior to mounting with Vectashield (Vector) mounting media. Leica's laser scanning SP5 microscope was used to acquire images. Image analysis was done with Imaris software (Bitplane AG) version 7 or higher.

Antibodies used include rabbit anti-MAEL [1:1,000 (Soper *et al*, 2008)], rabbit anti-ORF1p [1:1,000 (Martin & Branciforte, 1993)], mouse anti-γH2AX (Millipore, clone JBW301, 1:1,000), guinea pig anti-acrosomal protein mSP-10 [1:100, *Acrv1* (Reddi *et al*, 1995)], mouse anti-acetyl tubulin (1:200, Sigma Clone 6-11B-1). Secondary antibodies include Alexa 488 donkey anti-mouse (Molecular Probes A21202), Alexa 594 donkey anti-rabbit (Molecular Probes A21207), Alexa 488 donkey anti-rabbit (Molecular Probes A21206), Alexa 594 goat anti-guinea pig (Molecular Probes A11076) all used at 1:1,000.

Histology

For histological analyses, the slides were deparaffinized with xylene and hydrated through a series of decreasing percent of ethanol washes then with de-ionized water. Hematoxylin and eosin (H&E) or periodic acid–Schiff (PAS) staining was performed using standard protocols (Leblond & Clermont, 1952; Clermont & Perey, 1957; Russell *et al*, 1990). Slides were mounted with Vectamount (Vector) mounting media, and images were acquired with a Nikon Eclipse E800 microscope equipped with a Canon EOS Rebel T3i camera.

Electron microscopy

Specimens were fixed with glutaraldehyde/paraformaldehyde then osmium/ferricyanide in cacodylate buffer, dehydrated though graded ethanol then propylene oxide and embedded in epoxy resin. After polymerization, they were cut on a Leica ultramicrotome and photographed with a Gatan 794 camera mounted to an FEI Tecnai 12 electron microscope.

Coupling MAEL antibody to beads for immunoprecipitation (IP) for mass spectrometry and Western blot analysis

Rabbit anti-MAEL antibody (Soper *et al*, 2008) was coupled to an agarose resin using a commercially available kit (Thermo Scientific 26149).

Immunoprecipitation for mass spectrometry (MS)

IP analysis was done on testis lysate from CD1 wild-type and $Mael^{129-/-}$ adults. Testes from five wild-type CD1s and 16 $Mael^{129-/-}$ mice were dissected and homogenized with a Potter-Elvehjem homogenizer in 5 ml of an ice-cold Tris-based buffer (50 mM Tris pH 7.5, 150 mM NaCl, 0.1% NP-40 substitute, 1 mM DTT, Halt™ Protease and Phosphatase Inhibitors-EDTA free [Thermo Scientific], 1 mM PMSF, 100 U/ml RNasin). The lysates were clarified with two 10-min spins at 18,000 *g* at 4°C. The protein concentration was approximately 20 mg/ml for both lysates. The lysates volumes were adjusted to 10 ml with the same Tris-based buffer and incubated with anti-MAEL-coupled resin for 3 h at 4°C with gentle mixing. The mix was centrifuged for 2 min at 500 *g* at 4°C. The pellets were washed with approximately 1.6 ml of 50 mM Tris pH 7.5, 150 mM NaCl, 0.1% NP-40 substitute, and centrifuged for 1 min at 1,000 *g* at 4°C. The wash was repeated once more. The beads were then washed with 50 mM Tris pH 7.5, 150 mM NaCl twice in order to remove traces of NP-40 detergent for MS. The bound proteins were eluted off the beads with elution buffer from the co-IP Kit and centrifuged for 1 min at 1,500 *g* at room temperature. Two more subsequent elutions were performed. The elutions were then neutralized with 20 μl of 1 M Tris pH 9.0. A 20-μl aliquot was saved for SDS-PAGE analysis while the rest was stored at −80°C until preparation for MS submission. Elutions and washes were resolved on a 4–12% NuPAGE Gel (Invitrogen) and silver stained with the SilverQuest Staining kit (Invitrogen). For MS submission, samples were precipitated with 20% TCA, using 400 μg/ml of deoxycholate as a carrier, on ice for 10 min. The mix was centrifuged at 18,000 *g* for 15 min at 4°C. Pellets were washed with −20°C acetone and spun for 5 min at 18,000 *g* at 4°C. The acetone wash was repeated three more times to remove traces of deoxycholate. The MS analysis was performed by the Yates Lab (Scripps Institute) as described previously (Link *et al*, 1999).

Immunoprecipitations for Western blot analysis

For Western blot analysis, 25 μg of CD1 wild-type, 25 μg $Mael^{129-/-}$ adult testes lysates, and the TCA-precipitated elutions (wild-type and $Mael^{129-/-}$) were resolved on a 10% mini SDS-PAGE and transferred to a PVDF membrane. The PVDF membrane was blocked for 1 h with TBST containing 5% w/v non-fat dried milk. Primary antibodies were diluted with TBST containing 0.5% w/v non-fat dried milk and incubated with the membrane for 1 h at room temperature or overnight at 4°C. Secondary antibodies were diluted with TBST containing 0.5% w/v non-fat dry milk and incubated with the membrane for 1 h at room temperature. Four 5-min washes with TBST plus 0.5% w/v non-fat dried milk were performed after primary and secondary antibody incubations. Chemiluminescent detection was done with ECL Plus (GE Healthcare) or SuperSignal WestDura (Thermo Scientific) reagents.

Primary antibodies used for Western blot include the following: rabbit anti-MAEL (1:10,000), rabbit anti-MIWI (1:2,000 Abcam 12337), rabbit anti-TDRD6 [1:10,000 (Hosokawa *et al*, 2007)], rabbit anti-TDRD7 [1:10,000 (Hosokawa *et al*, 2007)], rabbit anti-TDRD9 [1:10,000 (Shoji *et al*, 2009)], rabbit anti-TDRD1 [1:10,000 (Hosokawa *et al*, 2007)], rabbit anti-RNF17/TDRD4 [1:2,000 (Pan *et al*, 2005)], rabbit anti-MILI (1:2,000 Abcam 367634), rabbit anti-actin

(1:1,000 Santa Cruz sc1615R), rabbit anti-MVH (1:10,000 Abcam 13840). Secondary antibodies used were HRP-conjugated anti-rabbit (GE Healthcare NA934, 1:5,000) and HRP-conjugated anti-mouse (GE Healthcare NX931, 1:5,000). For stripping and re-probing, membranes were incubated in 6 M guanidine, 20 mM Tris pH 7.5, 5 mM β-mercaptoethanol for 30 min at 4°C followed by five washes with PBS.

MAEL association with TDRD6, TDRD4, and MIWI proteins in cell culture

Full-length *Maelstrom* cDNA was cloned into the pTriEx-Hygro 1.1 (Novagen) vector or the pLP-EGFP-C1 (Clontech) vector. The HA-tagged *Tdrd6* (pcDNA3) construct was a kind gift from Ana Vasileva (Vasileva *et al*, 2009). GFP-tagged *Rnf17* and MYC-tagged *Miwi* pcDNA3 constructs were a kind gift from Jeremy Wang (Pan *et al*, 2005). HEK293T cells were subcultured with DMEM, 10% FBS, and Pen/Strep media (Gibco) on 100-mm cell culture plates. Transfections were carried out with Lipofectamine 2000 Reagent (Invitrogen). The cells were harvested 48 h after transfection and lysed by detergent lysis (50 mM Tris pH 7.5, 250 mM NaCl, 5 mM $MgCl_2$, 0.2% NP-40 substitute, 1 mM DTT, 100 U/ml RNasin, Halt™ Protease and Phosphatase Inhibitors-EDTA free, 1 mM PMSF) by gentle pipetting. Cell extracts were clarified by spinning at 18,000 *g* for 10 min at 4°C. Cell lysates were aliquoted, snap frozen, and stored at −80°C until use.

For IP from cell culture extracts, 50 μl of protein G sepharose beads (Roche) were incubated with 1 μg of antibody for 30 min at 4°C in 1 ml buffer (50 mM Tris pH 7.5, 150 mM NaCl, 5 mM $MgCl_2$, 0.1% NP-40 substitute). The antibody–bead mix was centrifuged at 1,500 *g* for 30 s at 4°C. 1 mg of lysate diluted with 1 ml buffer (50 mM Tris pH 7.5, 150 mM NaCl, 5 mM $MgCl_2$, 0.1% NP-40 substitute, 1 mM DTT, 100 U/ml RNasin, Halt™ Protease and Phosphatase Inhibitors-EDTA free, 1 mM PMSF) and was added to the pelleted beads. The mix was incubated for 1 h at 4°C. After the incubation, the beads were pelleted at 1,500 *g* for 30 s at 4°C. The beads were washed four times with 1 ml buffer (50 mM Tris pH 7.5, 150 mM NaCl, 5 mM $MgCl_2$, 0.1% NP-40 substitute). Proteins were eluted with 40 μl of 2× SDS–PAGE sample buffer then heating at 95°C for 5 min. For RNase treatment, RNase was added to a final concentration of 5 μg/ml.

Antibodies used for Western blot include rabbit anti-MAEL (1:10,000), mouse anti-HA (1:2,500 Sigma HA-7), mouse anti-FLAG (Sigma F1804, 1:5,000), mouse anti-MYC (Sigma 9E10, 1:5,000), rabbit anti-GFP (gift from Dr. Joseph Gall, 1:10,000).

Sucrose gradient preparation

Of 10–50% sucrose gradients were generated by layering 5% decreasing increments of sucrose solutions made with 20 mM HEPES pH 7.5, 100 mM KCl, 2 mM $MgCl_2$ (puromycin- and mock-treated samples), or 5 mM $MgCl_2$ (EDTA and untreated) in Ultra-Clear centrifuge tubes (Beckman 344059). Continuous gradients were obtained from the step gradients by the freeze–thaw method (Fourcroy *et al*, 1981; Luthe, 1983).

Velocity sedimentation analysis of MAEL

For preparing lysates for puromycin-treated (p+) or untreated (p−) samples, testes from one CD1 wild type were lysed in 1 ml ice-cold buffer [20 mM HEPES pH 7.5, 300 mM KCl, 2 mM $MgCl_2$, Halt™ Protease and Phosphatase Inhibitors-EDTA free, 1 mM DTT, 1% Triton X-100, 1 mM PMSF, and 500 μg/ml puromycin (p+) or 200 μg/ml cycloheximide (p−)] with a Potter-Elvehjem homogenizer. The lysates were clarified with a 10-min spin at 18,000 *g* at 4°C. 450 μl of supernatant was transferred to a new microcentrifuge tube and diluted 1:2 with 20 mM HEPES pH 7.5, 700 mM KCl, 2 mM $MgCl_2$, and 1% Triton X-100. SUPERaseIN (Invitrogen) and Turbo DNase (Invitrogen) were added to a final concentration of 100 and 5 U/ml, respectively. The lysates were incubated for 30 min at 37°C (Blobel & Sabatini, 1971; Ingolia *et al*, 2012), then one-half was layered on top of a 10–50% sucrose gradient. Centrifugation was carried out at 150,000 *g* for 3 h at 4°C. The gradients were fractionated over 18 fractions by collecting from the top with a P1000 pipette (~620 μl per fraction). Fraction #1 corresponds to the top of the gradient while #18 corresponds to the bottom of the gradient. Any potential pellet was dislodge from the tube by repeat pipetting and included in the last fraction (#18). The fractions were stored at −80°C.

Lysates for EDTA-treated (e+) or untreated (e−) samples were prepared as described for puromycin-treated/untreated samples with a few exceptions. 100 mM KCl was used for both samples. Untreated samples contained 5 mM $MgCl_2$ and 200 μg/ml cycloheximide while EDTA-treated contained 20 mM EDTA without cycloheximide. These lysates were not heat treated.

For Western blot analysis of the puromycin/untreated and EDTA/untreated samples, 100 μl of each fraction was precipitated with 20% TCA using 400 μg/ml deoxycholate as a carrier. The pellets were washed once with −20°C acetone. 40 μl of 2× SDS–PAGE sample buffer was used to resuspend the pellets. Only 15 μl was used for SDS-PAGE analysis. Proteins were resolved on a 10% SDS-PAGE and transferred to a PVDF membrane. Antibodies used for Western blot include rabbit anti-MAEL (1:10,000), rabbit anti-MIWI (1:2,000 Abcam 12337), rabbit anti-RPS6 (Novus NB100-1595, 1:5,000).

RT–PCR analysis of piRNA precursors in sucrose gradient fractions

RNA extraction from sucrose gradients

For RT–PCR analysis of the puromycin/mock and EDTA/untreated samples, RNA from 400 μl of each fraction was extracted with 600 μl of TRIzol (Invitrogen). The RNA pellets were resuspended in 10 μl of 10 mM Tris pH 8.0. Five microlitre of the resuspended pellet was used to assess rRNA sedimentation on a 1% agarose gel. The remaining 5 μl was used for RT–PCR analysis.

RT–PCR

For RT–PCR analysis, 5 μl of isolated RNA from the sucrose fractions was added to 9 μl of H_2O, 50 ng of random hexamer, and 1 μl of a 10 mM dNTP mix. The mix was heated to 65°C for 5 min in a thermocycler then chilled on ice for 2 min. 40 U of RNasin, 2 μl of 10× RT Buffer, and 200 U of MMLV Reverse Transcriptase (New England Biolabs, M0253L) was added to each sample. First-strand synthesis was carried out at 42°C for 1 h. Promega's GoTaq system was used for PCR. For PCR, we used 93°C 30-s denaturation, 60°C hybridization for 10 s, and 72°C 35-s extension, for 35 cycles. The primers used for Gapdh were 5′-ACCACAGTCCATGCCATCAC-3′ (forward)

and 5′-TCCACCACCCTGTTGCTGTA-3′ (reverse); for region #1 (chromosome 6:127759583-127760179), 5′-GACCTTTCCCTGTTTCCTCATCTTCC-3′ (forward) and 5′-TCGCCTTTGCCATAGGAGAATCAAG-3′ (reverse); for region #2 (chromosome 6:127760489-127761068), 5′-TTGTGGGGATTTGGGTTATACACAGAC (forward) and 5′-GCCCCAGGGTGACACTCTTGG (reverse); for region #3 (chromosome 6:127763176-127763465), 5′-AACCCACATAAACAAAAGCTCTTTGGG (forward) and 5′-GGTGGAGCATCCAAGAGATAGTTGG-3′ (reverse). PCR samples were run on a 2% agarose gel.

Sucrose gradient fractionation and RT–PCR analysis of candidate mRNAs

Continuous 10.8-ml 10–50% sucrose gradient was prepared as described above. Protein concentrations of testis lysates from 129 WT and *Mael*$^{-/-}$ adult mice were adjusted to be equal, and 400 μl (3.5 mg) was layered atop gradient columns. The absorbance at A260 of each fraction was measured using NanoDrop 2000 (Thermo Scientific). The RNA from each fraction was extracted using TRIzol reagent, and each two consecutive fractions were pooled to lower the number of analyzed samples. Precipitated RNA was diluted in appropriate buffer, treated with 6 U of Turbo DNase, purified with acid phenol–chloroform, precipitated, diluted in 10 mM Tris pH 8.0, and stored at −80°C. Equal volume of RNA from each fraction was used to prepare cDNA following SuperScript III First-Strand Synthesis System (Life Technologies) protocol with oligo (dT) primer. To prepare "−RT" control, reverse transcriptase was omitted from the reactions. The PCRs were setup in 96-well plates using 2 μl primer mix (5 μM each), 1/3 dilution of cDNA and amplified with GoTaq Polymerase (Promega) for 36 cycles in 20 μl reaction. Portion of each reaction (9 μl) was resolved on a 2% agarose gel and imaged using Gel Doc XR+ (Bio-Rad) with Image Lab 3.0 software. The intensities of bands in acquired tiff images were measured with ImageJ using the Gels feature. To directly compare WT and *Mael*$^{-/-}$ fractions, band intensities for same fraction were normalized by amount of their starting RNA. Finally, *Mael*$^{-/-}$ values were divided by the WT values yielding fold change in *Mael*$^{-/-}$. The primers used for *Gykl1* were 5′-GTGCTGAAGTCAATGGGTTG (forward) and 5′-AGGCATGATTTATGGGACACC (reverse), and for *Speer4d,* 5′-GCTGACCTTCCACCTGAGAGTAA (forward) and 5′-CTCAGCTCATTTGTCTCCTTGGT (reverse); for *Tekt4* 5′-TCGTGTGAGATGAACTGGTC (forward) and 5′- GGTTGTCGTGATTGAACTTGG (reverse); for *Zpbp2* 5′-GCTGTTCATAGCCTTTCAAGTG (forward) and 5′-GTTGAAGTGATGGTGTAGAATGTG (reverse).

Immunoprecipitation of MAEL for RNA-Seq

Immunoprecipitations for RNA-Seq

IPs were done on adult CD1 wild-type testis lysates. The lysates generated were prepared similarly as described for the lysates for MS analysis except that testes from 10 CD1s were homogenized in 8.5 ml of buffer with 5 mM $MgCl_2$ and 100 μg/ml cycloheximide. The protein concentration of lysate was approximately 10 mg/ml. approximately 500 μl of lysate was snap frozen and stored for RNA extraction at a later time point. 1.8 ml of protein lysate was incubated with each of the 500 μl of anti-MAEL or purified rabbit IgG (Sigma-Aldrich) coupled resin for 1 h at 4°C on a nutator. The beads were pelleted at 6,500 *g* for 30 s at 4°C. The beads were washed with approximately 2 ml of 50 mM Tris pH 7.5, 5 mM $MgCl_2$, 0.1% NP-40 substitute, 150 mM NaCl, and centrifuged at 6,500 *g* for 30 s at 4°C. The washes were repeated five more times. Two elutions were done using 500 μl of elution buffer. Elution samples were neutralized with 25 μl of 1 M Tris pH 9.0 and stored at −80°C.

RNA extraction and sequencing

RNA was extracted from 350 μl of lysate and 650 μl of the first elution from the MAEL IP and IgG IP with TRIzol. The RNA pellets were resuspended in 50 μl (RNA pellet from lysate) or 15 μl (RNA pellet from IP samples) of water. The RNA concentration from the lysate was measured using the NanoDrop 2000 while the RNA concentration from the IP samples was measured using the Eukaryotic Total RNA Pico kit (Agilent Technologies, 5067-1513) on a 2100 Bioanalyzer. Libraries for sequencing were generated using TrueSeq RNA Prep kit v2 (Illumina). Deep sequencing was carried out with Illumina's HiSeq2000 sequencer. Sequences were trimmed to remove 3′ adapter sequence (AGATCGGAAGAGCACAC), and trimmed reads were filtered to remove those aligning to a mouse rRNA database (Langmead *et al*, 2009). Filtered reads were aligned to the mouse genome (mm9) with Ensembl gene annotations (v67) combined with piRNA precursor transcript annotations (Li *et al*, 2013a,b) using the splicing-aware RNA-Seq aligner TopHat (Trapnell *et al*, 2009). Reads were also aligned to a database of transposable element consensus sequences (Langmead *et al*, 2009). The number of aligned reads was counted for 10-kb windows tiling the genome disjointedly, and on individual protein-coding and piRNA precursor transcripts. Regions (windows or transcripts) containing at least 100 total mapped reads across the two MAEL IP total RNA-Seq samples and the IgG control were selected for analysis of enrichment ratios. This included 25,534 genomic windows and 7,687 transcripts. Pairwise comparisons between samples were performed by finding the median enrichment ratio across all regions of detectable coverage to normalize the raw read count ratio in each sample, such that the median region had a ratio of 1. The R/Bioconductor scripts used to perform these analyses and the data frames plotted by these scripts are provided in Supplementary Dataset S1.

mRNA sequencing

For mRNA deep sequencing, total RNA from 150 μl of testes lysate from the 200 μl of snap-frozen lysate generated during ribosome footprinting was extracted by adding H_2O up to 400 μl and using 600 μl of TRIzol. Five micrograms of total RNA was treated with the discontinued non-magnetic Ribo-Zero Gold kit (Epicentre RZC1046), prior to library generation. The libraries were generated using TrueSeq RNA Prep kit v2 (Illumina).

Small RNA sequencing

For small RNA deep sequencing, 16 μg of *Mael*$^{129+/+}$ and 10 μg *Mael*$^{129-/-}$ of total RNA extracted from the 150 μl of unused lysate from the ribosome footprinting were run on a 15% TBE–Urea gel, for 65 min, at 200 V. A section of gel corresponding to approximately 15–40 nucleotides was excised. The excised gel slice was crushed in a RNase-free tube, and 400 μl of RNA gel extraction buffer was added (300 mM NaOAc pH 5.5, 1.0 mM EDTA, 0.25% SDS). The samples were frozen on dry ice for 30 min and incubated at room temperature overnight with gentle mixing. The samples

were centrifuged at 18,000 *g* for 1 min at room temperature, and the supernatant was transferred to a new microcentrifuge tube. The RNA was precipitated with 500 μl of isopropanol and 10 μg of linear acrylamide. The RNA concentration was quantified with a Small RNA Kit (Agilent Technologies, 5067-1548) and 2100 Bioanalyzer. Five nanograms of gel purified small RNA was used to generate the sequencing library using ScriptMiner™ Small RNA-Seq Library Preparation kit (Epicentre, SMMP101212). In the protocol, the optional TAP reaction in Part 4.A was included. For di-tagged RNA purification (Part 4.C step 4), the di-tagged RNA was precipitated by bringing the volume to 90 μl, adding 10 μl of 3 M NaOAc, and 150 μl isopropanol. The samples were frozen on dry ice for 30 min and pelleted for 30 min at 18,000 *g* at 4°C. The pellets were resuspended in 5 μl 10 mM Tris pH 8.0 and run on a 15% TBE–Urea gel for 65 min at 200 V. A section of gel corresponding to approximately 50–80 nucleotides was excised using a single-stranded RNA ladder (New England Biolabs, N0364S) as a guide. RNA was extracted from the gel slice as described previously. The remainder of the ScripMiner protocol was followed. 18 PCR cycles were the optimum number of cycles. All deep sequencing was carried out with Illumina's HiSeq2000 sequencer. Sequences were processed and analyzed in the same manner as RNA immunoprecipitation data. The abundance of piRNAs was estimated from counting the number of 26–32 nt small RNA sequencing reads aligning to each transcript in two biological replicates of each genotype. These raw read counts were normalized to correct for differences in sequencing depth, and variation was estimated from the inter-replicate dispersion under the assumption of a negative binomial distribution, using DESeq. Per-genotype piRNA abundance estimates and inter-genotype abundance differences were calculated using DESeq as well. The R/Bioconductor scripts used to perform these analyses and the data frames plotted by these scripts are provided in Supplementary Dataset S1.

Ribosome footprinting

For ribosome footprinting, lysates were generated from three testes pairs from P21 *Mael*$^{129+/+}$ and from P21 *Mael*$^{129-/-}$ mice. The protocol used for ribosome footprinting is outlined in Ingolia *et al* (2012) with a few modifications. The testes were homogenized in 600 μl lysis buffer supplemented with Halt™ Protease and Phosphatase Inhibitors (Thermo Scientific), 1 mM PMSF, and 1 U/μl Murine RNase Inhibitor (New England Biolabs M0314S). The crude extract was clarified at 18,000 *g* for 10 min at 4°C. 300 μl was used for ribosome footprinting while the remaining lysate (~200 μl) was snap frozen and stored at −80°C. RNA from the ribosome pellets was extracted by resuspending in 500 μl of 1% SDS and adding 800 μl of TRIzol. 10 μg of extracted RNA was run on a 15% TBE–Urea gel, for 65 min, at 200 V. The remainder of the footprinting protocol was followed as described (Ingolia *et al*, 2012). Sequences were processed and analyzed in the same manner as RNA immunoprecipitation data, except the 3′ linker sequence for these samples, "Linker 1", is CTGTAGGCACCATCAAT.

Accession code

The data discussed in this publication have been deposited in NCBI's Gene Expression Omnibus (Edgar *et al*, 2002) and are accessible through GEO Series accession number GSE50983 (http://www.ncbi.nlm.nih.gov/geo/query/acc.cgi?acc=GSE50983).

Supplementary information for this article is available online: http://emboj.embopress.org

Acknowledgements

This work was supported by the endowment of Carnegie Institution for Science (AB and NTI), the Searle Scholars Program (NTI), and the National Institute of General Medical Studies (P41 GM103533) of the National Institutes of Health by a grant to T.N.D. entitled "Comprehensive Biology: Exploiting the Yeast Genome" (JRY). We thank Eugenia Dikovsky for assistance with the ROSNI experiment.

Author contributions

JC, NTI, and AB conceived the research. JC, GWvdH, and PG performed the research. NTI performed computational analysis. AS and JRY performed mass spectrometry. JC, NTI, PG, and AB analyzed the data and wrote the paper. All authors reviewed the paper.

Conflict of interest

The authors declare that they have no conflict of interest.

References

Abe K, Noce T (1997) A DEAD-family protein gene, Ddx4, encoding a murine homolog of *Drosophila* vasa maps to the distal end of mouse chromosome 13. *Mamma Genome* 8: 622–623

Akagi K, Li J, Stephens RM, Volfovsky N, Symer DE (2008) Extensive variation between inbred mouse strains due to endogenous L1 retrotransposition. *Genome Res* 18: 869–880

Aravin A, Gaidatzis D, Pfeffer S, Lagos-Quintana M, Landgraf P, Iovino N, Morris P, Brownstein MJ, Kuramochi-Miyagawa S, Nakano T, Chien M, Russo JJ, Ju J, Sheridan R, Sander C, Zavolan M, Tuschl T (2006) A novel class of small RNAs bind to MILI protein in mouse testes. *Nature* 442: 203–207

Aravin AA, Hannon GJ, Brennecke J (2007a) The Piwi-piRNA pathway provides an adaptive defense in the transposon arms race. *Science* 318: 761–764

Aravin AA, Sachidanandam R, Girard A, Fejes-Toth K, Hannon GJ (2007b) Developmentally regulated piRNA clusters implicate MILI in transposon control. *Science* 316: 744–747

Aravin AA, Bourc'his D (2008) Small RNA guides for *de novo* DNA methylation in mammalian germ cells. *Genes Dev* 22: 970–975

Aravin AA, Sachidanandam R, Bourc'his D, Schaefer C, Pezic D, Toth KF, Bestor T, Hannon GJ (2008) A piRNA pathway primed by individual transposons is linked to *de novo* DNA methylation in mice. *Mol Cell* 31: 785–799

Aravin AA, van der Heijden GW, Castaneda J, Vagin VV, Hannon GJ, Bortvin A (2009) Cytoplasmic compartmentalization of the fetal piRNA pathway in mice. *PLoS Genet* 5: e1000764

Bingham JB, King SJ, Schroer TA (1998) Purification of dynactin and dynein from brain tissue. *Methods Enzymol* 298: 171–184

Blobel G, Sabatini D (1971) Dissociation of mammalian polyribosomes into subunits by puromycin. *Proc Natl Acad Sci USA* 68: 390–394

Bourc'his D, Bestor TH (2004) Meiotic catastrophe and retrotransposon reactivation in male germ cells lacking Dnmt3L. *Nature* 431: 96–99

Carmell MA, Girard A, van de Kant HJ, Bourc'his D, Bestor TH, de Rooij DG, Hannon GJ (2007) MIWI2 is essential for spermatogenesis and repression of transposons in the mouse male germline. *Dev Cell* 12: 503 – 514

Chuma S, Hiyoshi M, Yamamoto A, Hosokawa M, Takamune K, Nakatsuji N (2003) Mouse Tudor repeat-1 (MTR-1) is a novel component of chromatoid bodies/nuages in male germ cells and forms a complex with snRNPs. *Mech Dev* 120: 979 – 990

Chuma S, Hosokawa M, Kitamura K, Kasai S, Fujioka M, Hiyoshi M, Takamune K, Noce T, Nakatsuji N (2006) Tdrd1/Mtr-1, a tudor-related gene, is essential for male germ-cell differentiation and nuage/germinal granule formation in mice. *Proc Natl Acad Sci USA* 103: 15894 – 15899

Clermont Y, Perey B (1957) The stages of the cycle of the seminiferous epithelium of the rat: practical definitions in PA-Schiff-hematoxylin and hematoxylin-eosin stained sections. *Rev Can Biol* 16: 451 – 462

Costa Y, Speed RM, Gautier P, Semple CA, Maratou K, Turner JM, Cooke HJ (2006) Mouse MAELSTROM: the link between meiotic silencing of unsynapsed chromatin and microRNA pathway? *Hum Mol Genet* 15: 2324 – 2334

Deng W, Lin H (2002) Miwi, a murine homolog of piwi, encodes a cytoplasmic protein essential for spermatogenesis. *Dev Cell* 2: 819 – 830

Di Giacomo M, Comazzetto S, Saini H, De Fazio S, Carrieri C, Morgan M, Vasiliauskaite L, Benes V, Enright AJ, O'Carroll D (2013) Multiple epigenetic mechanisms and the piRNA pathway enforce LINE1 silencing during adult spermatogenesis. *Mol Cell* 50: 601 – 608

Doetschman T (2009) Influence of genetic background on genetically engineered mouse phenotypes. *Methods Mol Biol* 530: 423 – 433

Eaker S, Cobb J, Pyle A, Handel MA (2002) Meiotic prophase abnormalities and metaphase cell death in MLH1-deficient mouse spermatocytes: insights into regulation of spermatogenic progress. *Dev Biol* 249: 85 – 95

Edgar R, Domrachev M, Lash AE (2002) Gene expression omnibus: NCBI gene expression and hybridization array data repository. *Nucleic Acids Res* 30: 207 – 210

Findley SD, Tamanaha M, Clegg NJ, Ruohola-Baker H (2003) Maelstrom, a *Drosophila* spindle-class gene, encodes a protein that colocalizes with Vasa and RDE1/AGO1 homolog, Aubergine, in nuage. *Development* 130: 859 – 871

Fourcroy P, Cuiller S, Largitte FC, Lambert C (1981) Polyribosome analysis on sucrose gradients produced by the freeze-thaw method. *J Biochem Biophys Methods* 4: 243 – 246

Girard A, Sachidanandam R, Hannon GJ, Carmell MA (2006) A germline-specific class of small RNAs binds mammalian Piwi proteins. *Nature* 442: 199 – 202

Grivna ST, Beyret E, Wang Z, Lin H (2006a) A novel class of small RNAs in mouse spermatogenic cells. *Genes Dev* 20: 1709 – 1714

Grivna ST, Pyhtila B, Lin H (2006b) MIWI associates with translational machinery and PIWI-interacting RNAs (piRNAs) in regulating spermatogenesis. *Proc Natl Acad Sci USA* 103: 13415 – 13420

van der Heijden GW, Derijck AA, Posfai E, Giele M, Pelczar P, Ramos L, Wansink DG, van der Vlag J, Peters AH, de Boer P (2007) Chromosome-wide nucleosome replacement and H3.3 incorporation during mammalian meiotic sex chromosome inactivation. *Nat Genet* 39: 251 – 258

van der Heijden GW, Bortvin A (2009a) Defending the genome in tudor style. *Dev Cell* 17: 745 – 746

van der Heijden GW, Bortvin A (2009b) Transient relaxation of transposon silencing at the onset of mammalian meiosis. *Epigenetics* 4: 76 – 79

Hosokawa M, Shoji M, Kitamura K, Tanaka T, Noce T, Chuma S, Nakatsuji N (2007) Tudor-related proteins TDRD1/MTR-1, TDRD6 and TDRD7/TRAP: domain composition, intracellular localization, and function in male germ cells in mice. *Dev Biol* 301: 38 – 52

Huang H, Gao Q, Peng X, Choi SY, Sarma K, Ren H, Morris AJ, Frohman MA (2011) piRNA-associated germline nuage formation and spermatogenesis require MitoPLD profusogenic mitochondrial-surface lipid signaling. *Dev Cell* 20: 376 – 387

Ingolia NT, Ghaemmaghami S, Newman JR, Weissman JS (2009) Genome-wide analysis *in vivo* of translation with nucleotide resolution using ribosome profiling. *Science* 324: 218 – 223

Ingolia NT, Brar GA, Rouskin S, McGeachy AM, Weissman JS (2012) The ribosome profiling strategy for monitoring translation *in vivo* by deep sequencing of ribosome-protected mRNA fragments. *Nat Protoc* 7: 1534 – 1550

Ingolia NT (2014) Ribosome profiling: new views of translation, from single codons to genome scale. *Nat Rev Genet* 15: 205 – 213

Ipsaro JJ, Haase AD, Knott SR, Joshua-Tor L, Hannon GJ (2012) The structural biochemistry of Zucchini implicates it as a nuclease in piRNA biogenesis. *Nature* 491: 279 – 283

King SJ, Bonilla M, Rodgers ME, Schroer TA (2002) Subunit organization in cytoplasmic dynein subcomplexes. *Protein Sci* 11: 1239 – 1250

Kirino Y, Vourekas A, Sayed N, de Lima Alves F, Thomson T, Lasko P, Rappsilber J, Jongens TA, Mourelatos Z (2010) Arginine methylation of Aubergine mediates Tudor binding and germ plasm localization. *RNA* 16: 70 – 78

Kojima K, Kuramochi-Miyagawa S, Chuma S, Tanaka T, Nakatsuji N, Kimura T, Nakano T (2009) Associations between PIWI proteins and TDRD1/MTR-1 are critical for integrated subcellular localization in murine male germ cells. *Genes Cells* 14: 1155 – 1165

Kotaja N, Lin H, Parvinen M, Sassone-Corsi P (2006) Interplay of PIWI/Argonaute protein MIWI and kinesin KIF17b in chromatoid bodies of male germ cells. *J Cell Sci* 119: 2819 – 2825

Kuramochi-Miyagawa S, Kimura T, Ijiri TW, Isobe T, Asada N, Fujita Y, Ikawa M, Iwai N, Okabe M, Deng W, Lin H, Matsuda Y, Nakano T (2004) Mili, a mammalian member of piwi family gene, is essential for spermatogenesis. *Development* 131: 839 – 849

Kuramochi-Miyagawa S, Watanabe T, Gotoh K, Totoki Y, Toyoda A, Ikawa M, Asada N, Kojima K, Yamaguchi Y, Ijiri TW, Hata K, Li E, Matsuda Y, Kimura T, Okabe M, Sakaki Y, Sasaki H, Nakano T (2008) DNA methylation of retrotransposon genes is regulated by Piwi family members MILI and MIWI2 in murine fetal testes. *Genes Dev* 22: 908 – 917

Kuramochi-Miyagawa S, Watanabe T, Gotoh K, Takamatsu K, Chuma S, Kojima-Kita K, Shiromoto Y, Asada N, Toyoda A, Fujiyama A, Totoki Y, Shibata T, Kimura T, Nakatsuji N, Noce T, Sasaki H, Nakano T (2010) MVH in piRNA processing and gene silencing of retrotransposons. *Genes Dev* 24: 887 – 892

Langmead B, Trapnell C, Pop M, Salzberg SL (2009) Ultrafast and memory-efficient alignment of short DNA sequences to the human genome. *Genome Biol* 10: R25

Leblond CP, Clermont Y (1952) Spermiogenesis of rat, mouse, hamster and guinea pig as revealed by the periodic acid-fuchsin sulfurous acid technique. *Am J Anat* 90: 167 – 215

Lees-Murdock DJ, Walsh CP (2008) DNA methylation reprogramming in the germ line. *Epigenetics* 3: 5 – 13

Lerner EA, Lerner MR, Janeway CA Jr, Steitz JA (1981) Monoclonal antibodies to nucleic acid-containing cellular constituents: probes for

molecular biology and autoimmune disease. *Proc Natl Acad Sci USA* 78: 2737 – 2741

Li XZ, Roy CK, Dong X, Bolcun-Filas E, Wang J, Han BW, Xu J, Moore MJ, Schimenti JC, Weng Z, Zamore PD (2013a) An ancient transcription factor initiates the burst of piRNA production during early meiosis in mouse testes. *Mol Cell* 50: 67 – 81

Li XZ, Roy CK, Moore MJ, Zamore PD (2013b) Defining piRNA primary transcripts. *Cell Cycle* 12: 1657 – 1658

Link AJ, Eng J, Schieltz DM, Carmack E, Mize GJ, Morris DR, Garvik BM, Yates JR III (1999) Direct analysis of protein complexes using mass spectrometry. *Nat Biotechnol* 17: 676 – 682

Luthe DS (1983) A simple technique for the preparation and storage of sucrose gradients. *Anal Biochem* 135: 230 – 232

Ma L, Buchold GM, Greenbaum MP, Roy A, Burns KH, Zhu H, Han DY, Harris RA, Coarfa C, Gunaratne PH, Yan W, Matzuk MM (2009) GASZ is essential for male meiosis and suppression of retrotransposon expression in the male germline. *PLoS Genet* 5: e1000635

Martin SL, Branciforte D (1993) Synchronous expression of LINE-1 RNA and protein in mouse embryonal carcinoma cells. *Mol Cell Biol* 13: 5383 – 5392

Moens PB (1995) Histones H1 and H4 of surface-spread meiotic chromosomes. *Chromosoma* 104: 169 – 174

Newton I, Rinke J, Brimacombe R (1975) Random exchange of ribosomal proteins in EDTA sub-particles. *FEBS Lett* 51: 215 – 218

Nishimasu H, Ishizu H, Saito K, Fukuhara S, Kamatani MK, Bonnefond L, Matsumoto N, Nishizawa T, Nakanaga K, Aoki J, Ishitani R, Siomi H, Siomi MC, Nureki O (2012) Structure and function of Zucchini endoribonuclease in piRNA biogenesis. *Nature* 491: 284 – 287

Ogura A, Matsuda J, Yanagimachi R (1994) Birth of normal young after electrofusion of mouse oocytes with round spermatids. *Proc Natl Acad Sci USA* 91: 7460 – 7462

Pan J, Goodheart M, Chuma S, Nakatsuji N, Page DC, Wang PJ (2005) RNF17, a component of the mammalian germ cell nuage, is essential for spermiogenesis. *Development* 132: 4029 – 4039

Pek JW, Lim AK, Kai T (2009) Drosophila maelstrom ensures proper germline stem cell lineage differentiation by repressing microRNA-7. *Dev Cell* 17: 417 – 424

Pek JW, Anand A, Kai T (2012) Tudor domain proteins in development. *Development* 139: 2255 – 2266

Pillai RS, Chuma S (2012) piRNAs and their involvement in male germline development in mice. *Dev Growth Differ* 54: 78 – 92

Reddi PP, Naaby-Hansen S, Aguolnik I, Tsai JY, Silver LM, Flickinger CJ, Herr JC (1995) Complementary deoxyribonucleic acid cloning and characterization of mSP-10: the mouse homologue of human acrosomal protein SP-10. *Biol Reprod* 53: 873 – 881

Reuter M, Chuma S, Tanaka T, Franz T, Stark A, Pillai RS (2009) Loss of the Mili-interacting Tudor domain-containing protein-1 activates transposons and alters the Mili-associated small RNA profile. *Nat Struct Mol Biol* 16: 639 – 646

Reuter M, Berninger P, Chuma S, Shah H, Hosokawa M, Funaya C, Antony C, Sachidanandam R, Pillai RS (2011) Miwi catalysis is required for piRNA amplification-independent LINE1 transposon silencing. *Nature* 480: 264 – 267

Russell LD, Ettlin RA, SinhaHikim AP, Clegg ED (1990) *Histological and Histopathological Evaluation of the Testis*. St. Louis, MO: Cache River Press

Sanford LP, Kallapur S, Ormsby I, Doetschman T (2001) Influence of genetic background on knockout mouse phenotypes. *Methods Mol Biol* 158: 217 – 225

Sato K, Nishida KM, Shibuya A, Siomi MC, Siomi H (2011) Maelstrom coordinates microtubule organization during Drosophila oogenesis through interaction with components of the MTOC. *Genes Dev* 25: 2361 – 2373

Saxe JP, Chen M, Zhao H, Lin H (2013) Tdrkh is essential for spermatogenesis and participates in primary piRNA biogenesis in the germline. *EMBO J* 32: 1869 – 1885

Shoji M, Tanaka T, Hosokawa M, Reuter M, Stark A, Kato Y, Kondoh G, Okawa K, Chujo T, Suzuki T, Hata K, Martin SL, Noce T, Kuramochi-Miyagawa S, Nakano T, Sasaki H, Pillai RS, Nakatsuji N, Chuma S (2009) The TDRD9-MIWI2 complex is essential for piRNA-mediated retrotransposon silencing in the mouse male germline. *Dev Cell* 17: 775 – 787

Sienski G, Donertas D, Brennecke J (2012) Transcriptional silencing of transposons by piwi and maelstrom and its impact on chromatin state and gene expression. *Cell* 151: 964 – 980

Siomi MC, Sato K, Pezic D, Aravin AA (2011) PIWI-interacting small RNAs: the vanguard of genome defence. *Nat Rev Mol Cell Biol* 12: 246 – 258

Soper SF, van der Heijden GW, Hardiman TC, Goodheart M, Martin SL, de Boer P, Bortvin A (2008) Mouse maelstrom, a component of nuage, is essential for spermatogenesis and transposon repression in meiosis. *Dev Cell* 15: 285 – 297

Spirin AS (1974) Structural transformations of ribosomes (dissociation, unfolding and disassembly). *FEBS Lett* 40(Suppl.): S38 – S47

Tanaka T, Hosokawa M, Vagin VV, Reuter M, Hayashi E, Mochizuki AL, Kitamura K, Yamanaka H, Kondoh G, Okawa K, Kuramochi-Miyagawa S, Nakano T, Sachidanandam R, Hannon GJ, Pillai RS, Nakatsuji N, Chuma S (2011) Tudor domain containing 7 (Tdrd7) is essential for dynamic ribonucleoprotein (RNP) remodeling of chromatoid bodies during spermatogenesis. *Proc Natl Acad Sci USA* 108: 10579 – 10584

Trapnell C, Pachter L, Salzberg SL (2009) TopHat: discovering splice junctions with RNA-Seq. *Bioinformatics* 25: 1105 – 1111

Vagin VV, Wohlschlegel J, Qu J, Jonsson Z, Huang X, Chuma S, Girard A, Sachidanandam R, Hannon GJ, Aravin AA (2009) Proteomic analysis of murine Piwi proteins reveals a role for arginine methylation in specifying interaction with Tudor family members. *Genes Dev* 23: 1749 – 1762

Vasileva A, Tiedau D, Firooznia A, Muller-Reichert T, Jessberger R (2009) Tdrd6 is required for spermiogenesis, chromatoid body architecture, and regulation of miRNA expression. *Curr Biol* 19: 630 – 639

Vourekas A, Kirino Y, Mourelatos Z (2010) Elective affinities: a Tudor-Aubergine tale of germline partnership. *Genes Dev* 24: 1963 – 1966

Vourekas A, Zheng Q, Alexiou P, Maragkakis M, Kirino Y, Gregory BD, Mourelatos Z (2012) Mili and Miwi target RNA repertoire reveals piRNA biogenesis and function of Miwi in spermiogenesis. *Nat Struct Mol Biol* 19: 773 – 781

Vranis NM, van der Heijden GW, Malki S, Bortvin A (2010) Synaptonemal complex length variation in wild-type male mice. *Genes* 1: 505 – 520

Watanabe T, Takeda A, Tsukiyama T, Mise K, Okuno T, Sasaki H, Minami N, Imai H (2006) Identification and characterization of two novel classes of small RNAs in the mouse germline: retrotransposon-derived siRNAs in oocytes and germline small RNAs in testes. *Genes Dev* 20: 1732 – 1743

Watanabe T, Chuma S, Yamamoto Y, Kuramochi-Miyagawa S, Totoki Y, Toyoda A, Hoki Y, Fujiyama A, Shibata T, Sado T, Noce T, Nakano T, Nakatsuji N, Lin H, Sasaki H (2011) MITOPLD is a mitochondrial protein essential for nuage formation and piRNA biogenesis in the mouse germline. *Dev Cell* 20: 364 – 375

Yabuta Y, Ohta H, Abe T, Kurimoto K, Chuma S, Saitou M (2011) TDRD5 is required for retrotransposon silencing, chromatoid body assembly, and spermiogenesis in mice. *J Cell Biol* 192: 781 – 795

Yanagimachi R, Wakayama T, Kishikawa H, Fimia GM, Monaco L, Sassone-Corsi P (2004) Production of fertile offspring from genetically infertile male mice. *Proc Natl Acad Sci USA* 101: 1691 – 1695

Zhang D, Xiong H, Shan J, Xia X, Trudeau VL (2008) Functional insight into Maelstrom in the germline piRNA pathway: a unique domain homologous to the DnaQ-H 3′-5′ exonuclease, its lineage-specific expansion/loss and evolutionarily active site switch. *Biol Direct* 3: 48

Zhao S, Gou LT, Zhang M, Zu LD, Hua MM, Hua Y, Shi HJ, Li Y, Li J, Li D, Wang ED, Liu MF (2013) piRNA-triggered MIWI ubiquitination and removal by APC/C in late spermatogenesis. *Dev Cell* 24: 13 – 25

Zheng Q, Wang XJ (2008) GOEAST: a web-based software toolkit for Gene Ontology enrichment analysis. *Nucleic Acids Res* 36: W358 – W363

Zheng K, Wang PJ (2012) Blockade of pachytene piRNA biogenesis reveals a novel requirement for maintaining post-meiotic germline genome integrity. *PLoS Genet* 8: e1003038